IOP PUBLISHING JOURNAL OF PHYSICS D: APPLIED PHYSICS

J. Phys. D: Appl. Phys. **44** (2011) 395302 (22pp) doi:10.1088/0022-3727/44/39/395302

Influence of material ductility and crack surface roughness on fracture instability

Hamed Khezrzadeh[1], **Michael P Wnuk**[2] **and Arash Yavari**[3]

[1] Department of Civil Engineering, Center of Excellence in Structures and Earthquake Engineering, Sharif University of Technology, PO Box 11155-9313, Tehran, Iran
[2] College of Engineering and Applied Science, University of Wisconsin-Milwaukee, WI 53201, USA
[3] School of Civil and Environmental Engineering, Georgia Institute of Technology, Atlanta, GA 30332, USA

E-mail: arash.yavari@ce.gatech.edu

Received 16 March 2011, in final form 12 August 2011
Published 13 September 2011
Online at stacks.iop.org/JPhysD/44/395302

Abstract

This paper presents a stability analysis for fractal cracks. First, the Westergaard stress functions are proposed for semi-infinite and finite smooth cracks embedded in the stress fields associated with the corresponding self-affine fractal cracks. These new stress functions satisfy all the required boundary conditions and according to Wnuk and Yavari's (2003 *Eng. Fract. Mech.* **70** 1659–74) *embedded crack model* they are used to derive the stress and displacement fields generated around a fractal crack. These results are then used in conjunction with the *final stretch criterion* to study the quasi-static stable crack extension, which in ductile materials precedes the global failure. The material resistance curves are determined by solving certain nonlinear differential equations and then employed in predicting the stress levels at the onset of stable crack growth and at the critical point, where a transition to the catastrophic failure occurs. It is shown that the incorporation of the fractal geometry into the crack model, i.e. accounting for the roughness of the crack surfaces, results in (1) higher threshold levels of the material resistance to crack propagation and (2) higher levels of the critical stresses associated with the onset of catastrophic fracture. While the process of quasi-static stable crack growth (SCG) is viewed as a sequence of local instability states, the terminal instability attained at the end of this process is identified with the global instability. The phenomenon of SCG can be used as an early warning sign in fracture detection and prevention.

(Some figures in this article are in colour only in the electronic version)

1. Introduction

The phenomenon of slow stable crack extension or subcritical crack growth so ubiquitous in ductile and quasi-brittle fracture is not addressed in Griffith's theory of brittle fracture. Ultimately the analysis of this process leads to solutions for advancing cracks, which significantly differ from those valid for stationary cracks. The effect has been clearly noted in the antiplane case where continued crack advance is predicted under increasing load, and fracture appears as an instability in the process (Hult and McClintock 1956, McClintock 1958, McClintock and Irwin 1965). It has been shown that this instability behaviour from McClintock's antiplane analysis can be formulated in terms of a universal resistance curve, much as proposed by Krafft *et al* (1961). Physically this type of continuing crack growth resembles time-dependent or creep fracture observed in polymers. Studies on the microstructural level of ductile fracture occurring in metals and metallic alloys have brought up certain new mechanisms facilitating such growth as a sequence of debonding of the hard inclusions, followed by the formation of voids and their plastic deformation, growth and coalescence (Rice 1968). Rice also noticed that stable crack extension preceding instability is to be expected from the incremental and path-dependent nature of the plastic stress–strain relations such as those given by the Prandtl–Reuss relations.

Since elasto-plastic stress–strain relations are incremental in nature and path dependent, the analysis based on the continuum theory of plasticity (e.g. incremental flow theory

of Prandtl–Reuss) is extremely difficult if feasible at all (Gross 1990). There are only two exceptions to this statement, namely, antiplane exact formulation by Hult and McClintock (1956) and for the tensile fracture—analysis of Prandtl slip lines field generated in front of a crack advancing in a rigid-perfectly plastic solid (Rice and Sorensen 1978, Rice *et al* 1980). Their governing differential equation, which defines the material resistance curve, is identical to the results of Wnuk (1972, 1974, 1990) derived via application of the 'cohesive' and then 'structured cohesive' crack model, see also Budiansky (1988) and Wnuk and Legat (2002). When within the equilibrium cohesive zone associated with a tensile crack a 'unit step growth' or 'process zone' is incorporated into the Barenblatt–Dugdale model, and when Wnuk's *final stretch criterion* of fracture initiation is employed, one can then apply such a novel 'structured cohesive' model for analysis of continuing crack growth as a viable alternative to the continuum approaches (which with very few exceptions are not available), compare Wnuk and Mura (1983). In this context the exact coincidence of the governing equations derived by Wnuk (1972) and that of Rice *et al* (1980) is rather encouraging. More recently, Le *et al* (2009) have connected the phenomenon of subcritical crack growth in inelastic solids to the scale effects in lifetime and structural strength statistics. These authors show that there would be no scale effect, observed experimentally, if the process of slow stable crack growth (SCG) was not accounted for.

Real fracture surfaces are rough and the traditional modelling of cracks as smooth surfaces is at best an approximation. It is a known experimental fact that cracks in solids have rough surfaces and this 'roughness' evolves while a crack propagates (mirror-mist-hackle transition phenomenon). Irregular curves (surfaces) appear in many natural phenomena and it turns out that in many cases these irregular (rough) objects have some hidden degree of order. A fractal is a very special irregular set that has specific properties under scaling transformations. Curiosity of some researchers and the quest for finding better fracture models motivated several studies on modelling rough fracture surfaces with fractals. The experimental works started in the 1980s (Mandelbrot *et al* 1984) and today there is an overwhelming amount of experimental evidence that cracks in real materials are fractals in a wide range of scales. Among the theoretical contributions we can mention Mosolov (1991), Gol'dshteĭn and Mosolov (1991), Gol'dshteĭn and Mosolov (1992), Balankin (1997), Borodich (1997), Cherepanov *et al* (1995), Xie (1989), Carpinteri (1994), Carpinteri and Chiaia (1996), Yavari (2002), Yavari *et al* (2000, 2002a, 2002b), Wnuk and Yavari (2003, 2005, 2008, 2009), Yavari and Khezrzadeh (2010). The main results of these and related studies were the influence of fractality on the stress singularity at the crack tip, appearance of new modes of fracture, possibility of crack propagation in uniform compression, crack roughening and the increase in the cohesive zone size. The results of the mathematical evaluations presented here are subject to certain limitations. First, the range of the roughness parameter α is to be restricted to the interval (0.40, 0.50), which means that the crack surfaces are of small or moderate ruggedness. Such limitation is dictated by the confines of the 'embedded crack model' of Wnuk and Yavari (2003) and the limit $\alpha \approx 0.40$ is justified independently by the phenomenon of crack branching described by Yavari and Khezrzadeh (2010). While there are no restrictions imposed on the material ductility ρ defined in (54), satisfaction of Barenblatt's condition of small cohesive zone versus crack length ($R \ll a$) is assumed throughout this paper.

The primary objective of crack stress field analysis is to obtain a characterization of the stress and strain fields in the close vicinity of a crack tip within which the progressive separation events occur. Characterization in terms of stress intensity factor K, assuming linear-elastic behaviour, only requires knowledge of stresses and strains close to the crack tip. However, studies of cracks often involve displacement calculations at some distance from the crack tip. Therefore, solutions of crack problems that permit stress and displacement calculations in a finite domain around the crack tip are of interest. One effective way to solve the plane elasticity problems is to use complex variables. Muskhelishvili (1933) noted certain analysis advantages in using complex variables in solving plane elasticity problems. He showed that the solution of plane elasticity problem, $\nabla^4\Phi = 0$, where Φ is Airy's stress function, is the real or the imaginary part of

$$F = z^*\phi(z) + \chi(z), \tag{1}$$

where $z = x + \mathrm{i}y$, $z^* = x - \mathrm{i}y$ and $\phi(z)$ and $\chi(z)$ are two arbitrary holomorphic functions. Westergaard (1939) for some special types of crack problems proposed a simpler one-function approach. Westergaard discussed several mode I crack problems that can be solved using the following form of solutions:

$$\Phi = \mathrm{Re}\,\bar{\bar{Z}} + y\mathrm{Im}\,\bar{Z}, \tag{2}$$

where $\bar{Z} = \frac{\mathrm{d}\bar{\bar{Z}}}{\mathrm{d}z}$, $Z = \frac{\mathrm{d}\bar{Z}}{\mathrm{d}z}$ and Z is the Westergaard stress function, which is holomorphic.

In this paper we will find general solutions for fractal cracks in mode I. To do so, first we will obtain the close tip solutions for fractal cracks. Then we find the stress functions for a semi-infinite fractal crack and a fractal crack of finite nominal length $2a$, which are both under point loads. After obtaining these general stress functions we will use them to obtain stress functions for some special cases, and then the corresponding stress intensity factors and crack opening displacements (CODs). The aim of this paper is to study the effect of ductility and roughness on fracture instability. We extend Wnuk's work to self-affine fractal cracks and will show that roughness has a profound effect on fracture instability.

This paper is organized as follows. In section 2 we review general formulae required for the stress and displacement fields analysis by the use of Westergaard stress functions. Then the Westergaard stress functions and smooth crack field analysis results for the cases of semi-infinite and finite cracks of length $2a$ are briefly reviewed. In section 3 we propose Westergaard stress functions for three fractal crack cases: near-tip fields case, semi-infinite case and finite crack case. Using these Westergaard stress functions we determine the stress and displacement fields using the *method of embedded crack* (Wnuk and Yavari 2003). The stress fields are then used to

determine the fractal stress intensity factors. In section 4 stability of crack propagation and different efforts in analysing it are discussed. Section 5 is devoted to extending the *final stretch criterion* of Wnuk (1972, 1974) for fractal cracks. Using this criterion we carry out a stability analysis for fractal cracks. We discuss the terminal instability state in section 6. Conclusions are given in section 7. Some of the required detailed formulae and expressions for the stability analysis are given in the appendix.

2. Stress and displacement fields of smooth cracks

If the elasticity problem can be arranged so that the crack of interest lies on a straight segment of the x-axis ($y = 0$) according to Westergaard (1939) the stresses and displacements can be obtained from the stress function $Z(z)$ as

$$\sigma_{xx} = \mathrm{Re}\, Z - y\mathrm{Im}\, Z', \qquad \sigma_{yy} = \mathrm{Re}\, Z + y\mathrm{Im}\, Z',$$
$$\sigma_{xy} = -y\mathrm{Re}\, Z' \tag{3}$$

and

$$4Gu = (k-1)\mathrm{Re}\, \bar{Z} + 2y\mathrm{Im}\, Z,$$
$$4Gv = (k+1)\mathrm{Im}\, \bar{Z} - 2y\mathrm{Re}\, Z, \tag{4}$$

where $Z = \frac{\mathrm{d}\bar{Z}}{\mathrm{d}z}$, $Z' = \frac{\mathrm{d}Z}{\mathrm{d}z}$ and $k = 3 - 4\nu$ for plane strain and $k = \frac{3-\nu}{1+\nu}$ for plane stress. The term $\frac{k+1}{4G}$, which appears in the COD calculations can be simplified to $2/E'$, where $E' = E/(1-\nu^2)$ for plane strain and $E' = E$ for plane stress. In the following the results for smooth cracks are reviewed and then fractal cracks are studied (figure 1). In each case we start with point loads as we are interested in having Green's functions.

2.1. A semi-infinite smooth crack

We start with the problem of a semi-infinite smooth crack loaded by a pair of point loads. This problem was solved by Irwin (1957), and later on Tada *et al* (1985) added more details to this solution and derived exact relations for the COD and displacements along $(0, y)$. The stress function for the case of loading a semi-infinite crack by a pair of point loads of magnitude P at the point $x = -s$ (figure 1(*a*) and $H = 1$) as given by Irwin (1957) reads

$$Z(z) = \frac{P}{\pi(z+s)}\sqrt{\frac{s}{z}}. \tag{5}$$

The COD resulting from this stress function has the following form:

$$v = \frac{2}{E'}\frac{P}{\pi}\ln\left|\frac{\sqrt{|x|}+\sqrt{s}}{\sqrt{|x|}-\sqrt{s}}\right| \qquad x < 0. \tag{6}$$

The stress function (5) is used as a Green's function for determining stress functions for different loading conditions on a semi-infinite smooth crack. For example, for the case of a semi-infinite smooth crack loaded by a uniform pressure p along the segment $-b < x < 0$ the stress function is simply obtained by integrating (5) multiplied by p with respect to x over the interval $[-b, 0]$. This yields the following stress function:

$$Z(z) = \frac{2p}{\pi}\left\{\sqrt{\frac{b}{z}} - \tan^{-1}\sqrt{\frac{b}{z}}\right\}. \tag{7}$$

The resulting COD calculated from the stress function (7) reads

$$v = \frac{2}{E'}\frac{2pb}{\pi}\left\{\sqrt{\frac{|x|}{b}} + \left(1+\frac{x}{b}\right)\frac{1}{2}\ln\left|\frac{\sqrt{|x|}+\sqrt{b}}{\sqrt{|x|}-\sqrt{b}}\right|\right\} \qquad x < 0. \tag{8}$$

The case of small-scale yielding can be easily obtained from the above results. If we denote the length of the yield zone ahead of the crack by R, and the restraining stress acting within this zone by σ_{Y}, for small-scale yielding case ($R \ll a$) the stress function (7) reads

$$Z(z) = \frac{2\sigma_{\mathrm{Y}}}{\pi}\tan^{-1}\sqrt{\frac{R}{z}}. \tag{9}$$

The COD at the beginning (mouth) of the yield zone is of interest in fracture mechanics and is called crack tip opening displacement (CTOD). The resulting CTOD, δ for small-scale yielding is $\delta = \frac{8\sigma_{\mathrm{Y}}R}{\pi E'}$ (Barenblatt 1962, Irwin 1969). The size of the yield zone is obtained from the finiteness condition, which yields the equilibrium length $R = \frac{\pi}{8}[\frac{K_{\mathrm{I}}^{\mathrm{applied}}}{\sigma_{\mathrm{Y}}}]^2$.

2.2. A finite smooth crack of length 2a

The stress function for the case of loading a crack of finite length $2a$ by two pairs of point loads of magnitude P at the points $x = \pm s$ (figure 1(*b*) and smooth crack for which $H = 1$) has the following form (Irwin 1957, 1958, Erdogan 1962, Sih 1962, 1964, Paris and Sih 1965):

$$Z(z) = \frac{2P}{\pi}\frac{\sqrt{a^2-s^2}}{(z^2-s^2)\sqrt{1-(a/z)^2}}. \tag{10}$$

The resulting COD from the above stress function reads

$$v = \frac{2}{E'}\frac{P}{\pi}\ln\left|\frac{\sqrt{a^2-x^2}+\sqrt{a^2-s^2}}{\sqrt{a^2-x^2}-\sqrt{a^2-s^2}}\right| \qquad |x| < 0. \tag{11}$$

The problem of a crack of length $2a$ in an infinite plate under tensile far-field stresses can be solved by superposition of two distinct problems: (i) an infinite plate without a crack under tensile stress σ applied on its boundaries and (ii) an infinite plate with free boundaries and a finite crack of length $2a$, which is loaded by uniform pressure σ on its faces. Superposing these two problems one reaches the following Westergaard stress function:

$$Z(z) = \frac{\sigma z}{\sqrt{z^2-a^2}}. \tag{12}$$

For more details see Burdekin and Stone (1966) and Anderson (2004).

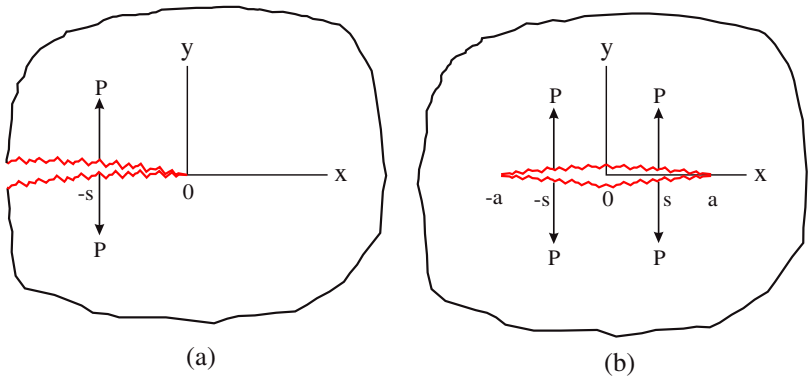

Figure 1. (*a*) A semi-infinite self-affine fractal crack loaded by a pair of point loads, (*b*) a self-affine fractal crack of finite nominal length $2a$ loaded by two pairs of point loads. Note that in the limit $H = 1$ these become their corresponding classical smooth cracks.

A cohesive crack. Let us consider a cohesive crack for which the lengths of the extended and physical cracks are $2c$ and $2a$, respectively. Stress function for constant tensile stress σ_Y applied along the cohesive zone is obtained again by integrating Green's function (10) over $a < |s| < c$, which for arbitrary R/c ratios yields

$$Z(z) = -\frac{2\sigma_Y}{\pi}\left[\frac{z}{\sqrt{(z^2-c^2)}}\cos^{-1}\left(\frac{a}{c}\right) - \tan^{-1}\left(\frac{z}{a}\sqrt{\frac{c^2-a^2}{z^2-c^2}}\right)\right]. \tag{13}$$

By superimposing the stress functions (12) and (13), the strip yield solution for the finite smooth crack is obtained. To do so we need to have the size of the cohesive zone ahead of the crack. As stated earlier, the size of the cohesive zone is chosen so that the stresses at the tips of the extended crack (of length $2a$) are finite, which corresponds to satisfying the finiteness condition: $K_I^{\text{applied}} + K_I^{\text{cohesive}} = 0$. The ratio of the size of the physical crack to the size of the extended crack (a/c) is obtained as

$$h = \frac{a}{c} = \cos\left(\frac{\pi\sigma}{2\sigma_Y}\right). \tag{14}$$

Now by substituting the ratio a/c in (12) and (13) and after some algebraic manipulations one reaches the following expression for the COD:

$$v = \frac{4\sigma_Y}{\pi E'}\left[a\coth^{-1}\left(\frac{1}{c}\sqrt{\frac{c^2-z^2}{1-h^2}}\right) - z\coth^{-1}\left(\frac{h}{z}\sqrt{\frac{c^2-z^2}{1-h^2}}\right)\right], \qquad |z| \leqslant c. \tag{15}$$

By substituting $z = a$ in the above equation the CTOD, δ is obtained as

$$\delta = \frac{8a\sigma_Y}{\pi E'}\ln\left(\frac{1}{h}\right). \tag{16}$$

When Barenblatt's condition $(c-a)/c \ll 1$ is satisfied, the expressions for the size of the cohesive zone and δ reduce to

$$\frac{c-a}{a} = \frac{1}{2}\left(\frac{\pi\sigma}{2\sigma_Y}\right)^2, \qquad \delta = \frac{8(c-a)\sigma_Y}{\pi E'}. \tag{17}$$

We will denote the size of the cohesive zone (i.e. $c-a$) by R throughout the paper.

3. Stress and displacement fields for fractal cracks

In the following we obtain approximate stress and displacement fields for fractal cracks by embedding an auxiliary smooth crack in the stress field of a fractal crack according to the method of *embedded crack* (Wnuk and Yavari 2003). We will then obtain the appropriate stress functions for this auxiliary smooth crack.

3.1. Near-tip solutions for a fractal crack

From many investigations on fractal cracks it has been found that the order of singularity of stress around a fractal crack tip is different from that of a smooth crack (Mosolov 1991, Gol'dshteĭn and Mosolov 1991, 1992, Balankin 1997, Yavari *et al* 2000, Yavari 2002, Yavari and Khezrzadeh 2010). The order of stress singularity for fractal cracks depends on the degree of roughness, which is quantified by the roughness (Hurst) exponent H for self-affine fractal cracks. The order of stress singularity α resulted from asymptotic analysis for a self-affine fractal crack reads $\alpha = \frac{2H-1}{2H}$ ($\frac{1}{2} < H \leqslant 1$). Throughout the paper we refer to α as 'roughness index' or 'fractality index'.

Asymptotic analysis gives important information about the dominant terms in the close vicinity of the crack tip; however, it cannot give the complete field solutions. As stated earlier, a complete field analysis requires an appropriate choice of stress functions. A stress function must satisfy some conditions and once it is found one can argue that it gives the unique solution of the problem because of the uniqueness of linear elasticity solutions. The stress function must satisfy the following conditions: (i) stress function must be singular of order α at the crack tip. (ii) The stress function must result in stress components with the correct physical dimensions. Because the order of stress singularity is different for fractal cracks special care must be taken in choosing a stress function. (iii) Any problem can be easily broken up into superposition of an infinite body with a crack that is loaded on its faces and has free boundaries and an infinite body without a crack that is loaded on its boundaries (far-field loading). What we are

interested in is the first problem. To satisfy the conditions of free boundaries at infinity for this problem it is required to have zero stresses for $z \to \infty$. (iv) On the crack faces traction vector must vanish. Because the stresses on the crack faces ($y = \pm 0$ and $x < 0$) depend only on the real part of $Z(z)$ (see (3)), the stress function must have a vanishing real part on the crack faces. (v) Because of symmetry, vertical displacements must be symmetric with respect to the x-axis. Therefore, for $x > 0$ on the x-axis the vertical displacement resulted from the stress function must be zero. By referring to (4) we find that this condition is satisfied if $\mathrm{Im}\,\bar{Z} = 0$. (vi) For $H = 1$ the stress function should be reduced to that of the corresponding smooth crack, which is (Williams (1957), Irwin (1958)): $Z(z) = \frac{K_{\mathrm{I}}}{\sqrt{2\pi z}}$. The stress function must also be a smooth function of roughness exponent H.

Considering the above conditions we propose the following stress function for the dominant term of the stress function around the tip of a fractal crack:

$$Z(z;\alpha) = \frac{1}{\mathrm{e}^{\mathrm{i}(\frac{1}{2}-\alpha)\theta}} \frac{K_{\mathrm{I}}^{\mathrm{f}}}{(2\pi z)^{\alpha}}. \tag{18}$$

In polar coordinates this reads $Z(r,\theta;\alpha) = \frac{K_{\mathrm{I}}^{\mathrm{f}}}{(2\pi r)^{\alpha}\mathrm{e}^{\mathrm{i}\theta/2}}$. It can be easily checked that this stress function satisfies all the above conditions. It should be noted that what we have suggested here is very similar to the close tip stress function proposed earlier in Wnuk and Yavari (2003). In fact, the only difference between the two expressions is the pre-factor $1/\mathrm{e}^{\mathrm{i}(\frac{1}{2}-\alpha)\theta}$. The expression proposed by Wnuk and Yavari (2003) is real-valued on the line ($x > 0$ and $y = 0$) and is identical to our stress function, but elsewhere it does not satisfy some of the required conditions of a stress function. For example, it gives both real and imaginary parts on the crack line ($x < 0$ and $y = 0$), which is not correct. In this new stress function the issues of the previous stress function of Wnuk and Yavari (2003) have been resolved by introducing a pre-factor. We will compare the two resulting stress intensity factors at the end of this section.

To find the stress field we need the derivative of the stress function (18), which reads

$$Z'(r,\theta;\alpha) = \frac{-\alpha}{r} \frac{K_{\mathrm{I}}^{\mathrm{f}}}{(2\pi r)^{\alpha}\mathrm{e}^{\mathrm{i}3\theta/2}}. \tag{19}$$

The terms that are needed to determine the stress field can be easily extracted from the above stress functions. These are

$$\mathrm{Re}\,Z = \frac{K_{\mathrm{I}}^{\mathrm{f}}}{(2\pi r)^{\alpha}}\cos\frac{\theta}{2}, \qquad \mathrm{Re}\,Z' = \frac{-\alpha}{r}\frac{K_{\mathrm{I}}^{\mathrm{f}}}{(2\pi r)^{\alpha}}\cos\frac{3\theta}{2},$$
$$\mathrm{Im}\,Z' = \frac{\alpha}{r}\frac{K_{\mathrm{I}}^{\mathrm{f}}}{(2\pi r)^{\alpha}}\sin\frac{3\theta}{2}. \tag{20}$$

Using (3), we obtain the following expressions for the stress distribution in the close vicinity of the crack tip

$$\sigma_{xx} = \frac{K_{\mathrm{I}}^{\mathrm{f}}}{(2\pi r)^{\alpha}}\left[\cos\frac{\theta}{2} - \alpha\sin\theta\sin\frac{3\theta}{2}\right],$$
$$\sigma_{yy} = \frac{K_{\mathrm{I}}^{\mathrm{f}}}{(2\pi r)^{\alpha}}\left[\cos\frac{\theta}{2} + \alpha\sin\theta\sin\frac{3\theta}{2}\right], \tag{21}$$
$$\sigma_{xy} = \frac{K_{\mathrm{I}}^{\mathrm{f}}}{(2\pi r)^{\alpha}}\alpha\sin\theta\cos\frac{3\theta}{2}.$$

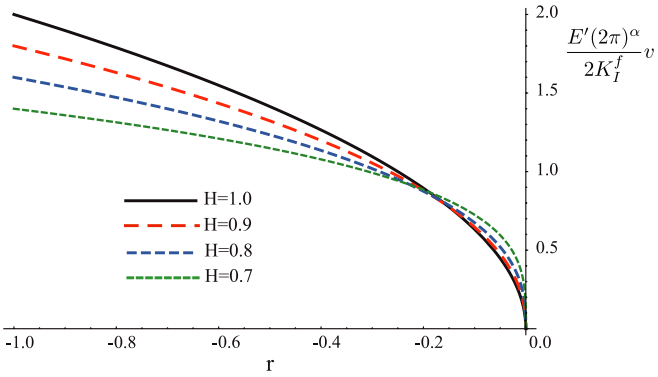

Figure 2. Normalized COD near the tip of a fractal crack for different values of roughness exponent H.

The stress components in polar coordinates read

$$\sigma_{rr} = \frac{K_{\mathrm{I}}^{\mathrm{f}}}{(2\pi r)^{\alpha}}(1+\alpha-\alpha\cos\theta)\cos\frac{\theta}{2},$$
$$\sigma_{\theta\theta} = \frac{K_{\mathrm{I}}^{\mathrm{f}}}{(2\pi r)^{\alpha}}(1-\alpha+\alpha\cos\theta)\cos\frac{\theta}{2}, \tag{22}$$
$$\sigma_{r\theta} = \frac{K_{\mathrm{I}}^{\mathrm{f}}}{(2\pi r)^{\alpha}}2\alpha\cos^2\frac{\theta}{2}\sin\frac{\theta}{2}.$$

In the following we will find the near-tip COD. We first need to find the antiderivative of (18).[4] To do so we rearrange the stress function (18) as follows:

$$Z(r,\theta;\alpha) = \frac{K_{\mathrm{I}}^{\mathrm{f}}\mathrm{e}^{\mathrm{i}\theta/2}}{(2\pi r)^{\alpha}}\mathrm{e}^{-\mathrm{i}\theta}. \tag{23}$$

Thus, $\bar{Z}(r,\theta;\alpha)$ reads

$$\bar{Z}(r,\theta;\alpha) = \frac{r^{1-\alpha}K_{\mathrm{I}}^{\mathrm{f}}\mathrm{e}^{\mathrm{i}\theta/2}}{(1-\alpha)(2\pi)^{\alpha}}. \tag{24}$$

By extracting the real and imaginary parts of the above equation on the crack face ($\theta = \pi$, $y = 0$) we obtain the following expression for the COD:

$$v = \frac{2K_{\mathrm{I}}^{\mathrm{f}}}{E'(2\pi)^{\alpha}}\frac{r^{1-\alpha}}{1-\alpha}. \tag{25}$$

As can be seen, the above COD reduces to its classical counterpart for a smooth crack ($\alpha = \frac{1}{2}$). As expected a weaker stress singularity results in smaller (normalized) close tip displacements (see figure 2).

3.2. A semi-infinite fractal crack

In this section we estimate the stress field around a semi-infinite fractal crack under a pair of point loads. To do so we again use the *method of embedded crack*. We obtain the stress functions for various types of loadings using this (Green's function) solution. The following conditions must

[4] Note that stress functions are analytic and single valued in the domain of interest ($-\pi < \theta < \pi$). The crack line is a branch cut in the complex plane. This means that all the integrals in the domain of analyticity of the stress functions are path independent.

be satisfied by the stress function: (i) stress function must be singular of order α at the crack tip and singular of order 1 at the loading point. (ii) Stress function must result in stress components with the correct physical dimensions. (iii) On the crack faces traction vector must vanish[5]. Because only the real part of $Z(z)$ contributes to stresses on the crack faces ($y = \pm 0$ and $x < 0$) (see (3)), the stress function must have a vanishing real part on the crack faces. (iv) Because of symmetry, vertical displacements must be symmetric with respect to the x-axis. Therefore, for $x > 0$ on the x-axis the vertical displacement resulted from the stress function must be zero. Referring to (4) we find that this condition is satisfied if $\operatorname{Im} \bar{Z} = 0$. (v) For $H = 1$ the stress function must be reduced to that of a smooth crack, i.e. (Irwin 1957, Tada *et al* 1985): $Z(z) = \frac{P}{\pi(z+s)}\sqrt{\frac{s}{z}}$.

Considering the above conditions we propose the following stress function for a semi-infinite fractal crack loaded by a pair of concentrated loads of magnitude P at a distance s from the crack tip:

$$Z(z;\alpha) = \frac{1}{e^{i(\frac{1}{2}-\alpha)\theta}} \frac{P}{\pi(z+s)} \frac{s^\alpha}{z^\alpha}. \tag{26}$$

Its antiderivative $\bar{Z}$ reads

$$\bar{Z}(z;\alpha) = \frac{P}{\pi(1-\alpha)} \frac{1}{e^{i(\frac{1}{2}-\alpha)\theta}} \times \left(\frac{z}{s}\right)^{1-\alpha} f\left(1-\alpha, 1, 2-\alpha; -\frac{z}{s}\right), \tag{27}$$

where

$$f(\phi, \chi, \psi; x) = \frac{\Gamma(\psi)}{\Gamma(\chi)\Gamma(\psi-\chi)} \times \int_0^1 t^{\chi-1}(1-t)^{\psi-\chi-1}(1-tx)^{-\phi} \mathrm{d}t, \qquad \psi > \chi > 0. \tag{28}$$

The real and imaginary parts of the above function cannot be easily obtained; we use Mathematica®. Green's function (26) can be used to determine stress functions in other loading conditions. For uniform pressure σ along the segment $-b < x < 0$ the stress function reads

$$\hat{Z}(z;\alpha) = \frac{\sigma}{\pi} \frac{1}{e^{i(\frac{1}{2}-\alpha)\theta}} \times \frac{1}{(1+\alpha)} \left(\frac{b}{z}\right)^{1+\alpha} f\left(1+\alpha, 1, 2+\alpha; -\frac{b}{z}\right). \tag{29}$$

The resulting normalized CODs are plotted in figure 3 for different values of roughness exponent H.

Stress functions can be used to obtain the stress intensity factors. The fractal stress intensity factor is defined as (Wnuk and Yavari 2003)

$$K_{\mathrm{I}}^{\mathrm{f}} = \lim_{\xi \to 0} (2\pi\xi)^\alpha \operatorname{Re} Z. \tag{30}$$

The stress intensity factor for the case of point loads of magnitude P applied at the point $x = -s$ of the semi-infinite fractal crack are obtained from the stress function (26) as follows:

$$K_{\mathrm{I}}^{\mathrm{f}} = \lim_{\xi \to 0} (2\pi\xi)^\alpha \operatorname{Re} Z = \lim_{\xi \to 0} (2\pi\xi)^\alpha \frac{P}{\pi(\xi+s)} \left(\frac{s}{\xi}\right)^\alpha = \frac{2^\alpha P}{(\pi s)^{1-\alpha}}. \tag{31}$$

This serves as a Green's function for other loading conditions, i.e. stress intensity factor from a general loading $p(x)$ can be simply obtained by integrating the above Green's function multiplied by $p(x)$, which gives

$$K_{\mathrm{I}}^{\mathrm{f}} = \int_{-\infty}^{0} \frac{2^\alpha p(x)}{(\pi|x|)^{1-\alpha}} \mathrm{d}x. \tag{32}$$

As an example, for the case of constant pressure loading σ^∞ along the segment $-b < x < 0$ we obtain the following stress intensity factor:

$$K_{\mathrm{I}}^{\mathrm{f}} = \int_{-b}^{0} \frac{2^\alpha \sigma^\infty \mathrm{d}x}{(\pi|x|)^{1-\alpha}} = \frac{2^\alpha \sigma^\infty b^\alpha}{\alpha \pi^{1-\alpha}}. \tag{33}$$

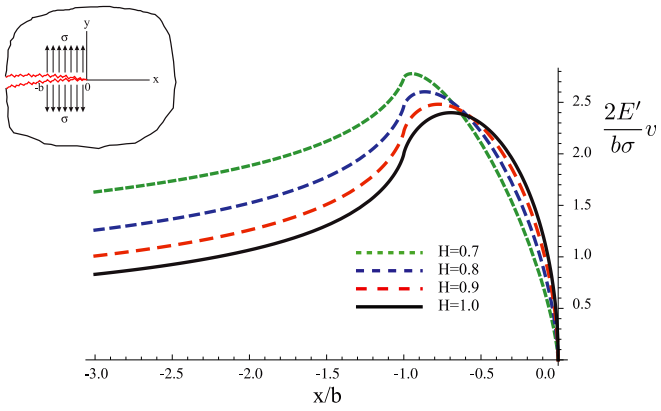

Figure 3. COD in a semi-infinite fractal crack under uniform pressure along the segment $-1 < x/b < 0$ for different values of roughness exponent H.

3.3. A fractal crack of finite nominal length 2a

In this section we estimate the stress field around the tip of a fractal crack of finite nominal length. The following conditions must be satisfied by the stress function: (i) Stress function is expected to be singular of order α at the crack tips and singular of order 1 at the loading points ($x = \pm s$). (ii) The stress function should result in stress components with the correct physical dimensions. (iii) On the crack faces traction vector should vanish. Because only the real part of $Z(z)$ contributes to stresses on the crack faces ($y = \pm 0$ and $-a < x < a$), the stress function must have a vanishing real part on the crack faces (see (3)). (iv) Because of symmetry, vertical displacements must be symmetric with respect to the x-axis. Therefore, for ($x > a$ and $x < -a$) on the x-axis the vertical displacement resulting from the stress function must be zero. By referring to (4) we find that this condition is satisfied when $\operatorname{Im} \bar{Z} = 0$. (v) For $H = 1$ the stress function should reduce to that of the corresponding smooth crack, which is (Irwin 1957,

[5] Note that in the close vicinity of the crack faces and at the point where the load is applied σ_{yy} is singular.

1958, Erdogan 1962, Sih 1962, 1964, Paris and Sih 1965)

$$Z(z) = \frac{2P}{\pi}\frac{\sqrt{a^2 - s^2}}{(z^2 - s^2)\sqrt{1 - (a/z)^2}}.$$

It is expected to be a continuous function of α or H.

Considering the above conditions we propose the following stress function for the case of symmetric loading by two pairs of concentrated forces P at the points $\pm s$:

$$Z(z;\alpha) = \frac{P}{\pi}\frac{1}{e^{i(\frac{1}{2}-\alpha)2|\pi/2-\theta|}}\frac{(a-s)^\alpha(a+s)^\alpha}{(z-a)^\alpha(z+a)^\alpha}\frac{2z}{z^2-s^2}. \tag{34}$$

It is easy to check that this stress function satisfies all the above conditions. Westergaard stress functions for different loading conditions on the finite fractal crack can be obtained using Green's function (34). If we denote the loading on the crack faces by $p(x)$, the corresponding Westergaard stress function is obtained as

$$Z(z;\alpha) = \frac{1}{e^{i(\frac{1}{2}-\alpha)2|\pi/2-\theta|}}\int_{-a}^{a}\frac{p(x)}{\pi(z-x)}\frac{(a^2-x^2)^\alpha}{(z^2-a^2)^\alpha}\,dx. \tag{35}$$

For the case of constant pressure σ^∞ along the segment $(a < |x| < c)$ the result of integration is

$$\begin{aligned}\hat{Z}(z;\alpha) = {} & \frac{\sigma^\infty}{e^{i(\frac{1}{2}-\alpha)2|\pi/2-\theta|}}\frac{1}{2(z^2-c^2)^\alpha}\left\{\frac{1}{\alpha}\left[\left(\frac{-1}{(a-z)^2}\right)^{-\alpha}\right.\right.\\ & \times g\left(-2\alpha,-\alpha,-\alpha,1-2\alpha,\frac{z+c}{z-a},\frac{z-c}{z-a}\right)\\ & -\left(\frac{-1}{(a+z)^2}\right)^{-\alpha}\\ & \left.\left.\times g\left(-2\alpha,-\alpha,-\alpha,1-2\alpha,\frac{z-c}{z+a},\frac{z+c}{z+a}\right)\right]\right.\\ & +2(-1)^\alpha\Gamma(-2\alpha)\Gamma(1+\alpha)\\ & \times\left[\left(\frac{1}{c-z}\right)^{-2\alpha}f\left(-2\alpha,-\alpha,1-\alpha,1+\frac{2c}{z-c}\right)\right.\\ & \left.\left.-\left(\frac{1}{c+z}\right)^{-2\alpha}f\left(-2\alpha,-\alpha,1-\alpha,1-\frac{2c}{z+c}\right)\right]\right\},\end{aligned} \tag{36}$$

where $f(\phi,\chi,\psi;x)$ was defined in (28) and $g(\phi,\chi_1,\chi_2,\psi;x,y)$ is the Appell hypergeometric function of two variables (Weisstein 2003, Slater 2008).

By definition the stress intensity factor for a fractal crack is related to the stress function (Wnuk and Yavari 2003):

$$K_{\mathrm{I}}^{\mathrm{f}} = \lim_{\xi\to a}[2\pi(\xi-a)]^\alpha\,\mathrm{Re}\,Z. \tag{37}$$

Hence, the fractal stress intensity factor is obtained from (35) as follows:

$$\begin{aligned}K_{\mathrm{I}}^{\mathrm{f}} &= \lim_{\xi\to a}[2\pi(\xi-a)]^\alpha\int_{-a}^{a}\frac{p(x)}{\pi(\xi-x)}\frac{(a^2-x^2)^\alpha}{(\xi^2-a^2)^\alpha}dx\\ &= \int_{-a}^{a}\frac{p(x)}{\pi^{1-\alpha}a^\alpha}\frac{(a+x)^\alpha}{(a-x)^{1-\alpha}}dx.\end{aligned} \tag{38}$$

Assuming an even distribution of pressure on the crack faces will result in the following fractal stress intensity factor:

$$\begin{aligned}K_{\mathrm{I}}^{\mathrm{f}} &= \int_a^0\frac{p(-x')}{\pi^{1-\alpha}a^\alpha}\frac{(a-x')^\alpha}{(a+x')^{1-\alpha}}(-dx')\\ &\quad+\int_0^a\frac{p(x)}{\pi^{1-\alpha}a^\alpha}\frac{(a+x)^\alpha}{(a-x)^{1-\alpha}}dx\\ &= \left(\frac{a}{\pi}\right)^{1-\alpha}\int_0^a\frac{2p(x)}{(a^2-x^2)^{1-\alpha}}dx.\end{aligned} \tag{39}$$

It should be noted that the above relation is just an approximation for the fractal stress intensity factor and increasing roughness its accuracy decreases. There is another approximation for the fractal stress intensity factor that was proposed earlier by Wnuk and Yavari (2003). To compare our results with the fractal stress intensity factor of Wnuk and Yavari (2003), we first simplify (39) for the case of uniform pressure. The resulting stress intensity factor for a fractal crack reads

$$K_{\mathrm{I}}^{\mathrm{f}} = \left(\frac{a}{\pi}\right)^{1-\alpha}\int_0^a\frac{2\sigma^\infty}{(a^2-x^2)^{1-\alpha}}dx = \frac{a^\alpha\pi^{\alpha-\frac{1}{2}}\Gamma(\alpha)\sigma^\infty}{\Gamma(\alpha+\frac{1}{2})}. \tag{40}$$

This can be rewritten as

$$K_{\mathrm{I}}^{\mathrm{f}} = \xi(\alpha)\sigma^\infty\sqrt{\pi a^{2\alpha}}, \tag{41}$$

where

$$\xi(\alpha) = \frac{\pi^{\alpha-1}\Gamma(\alpha)}{\Gamma(\alpha+\frac{1}{2})}. \tag{42}$$

The normalized results (with respect to $\sigma^\infty a^\alpha$) from the above relation and that of Wnuk and Yavari (2003) are plotted in figure 4. This new fractal stress intensity factor goes to infinity for $H = 0.5$ but it should be noted that since there exists a limiting roughness for a fractal crack[6], reaching such a highly irregular form is physically impossible. We should also note that the *method of embedded crack* is a good approximation only for moderately rough cracks. For moderately rough cracks within a considerable range of the fractality index α $(0.25 < \alpha < 0.5)$ the graphs in figure 4 show excellent agreement.

The reason for the difference between the two stress intensity factors. Let us now explain why our fractal stress intensity factor is different from that given by Wnuk and Yavari (2003). Wnuk and Yavari (2003) introduced a Westergaard stress function, which for $|x| > a$ and $y = 0$ is identical to our stress function (34). Then they used an approximation to determine the stress intensity factor, namely they defined the following function:

$$\hat{K}_{\mathrm{I}}^{\mathrm{f}} = \frac{1}{(\pi a)^\alpha}\int_{-a}^{a}p(x)\left[\frac{a+x}{a-x}\right]^\alpha dx. \tag{43}$$

[6] There are many researchers who argue that there exists a universal roughness for fracture surfaces. Their studies on the fracture surfaces of different materials indicate that for both quasi-static and dynamic fracture a universal roughness exponent (H) of approximate value 0.8 is observed for values of ξ (scale of observation) greater than a material-dependent scale, ξ_c (Bouchaud *et al* 1990, Måløy *et al* 1992, Daguier *et al* 1996, 1997, Bouchaud 1997, 2003, Ponson *et al* 2006). Recently, Yavari and Khezrzadeh (2010) using a branching argument showed that there is a limiting roughness and estimated it.

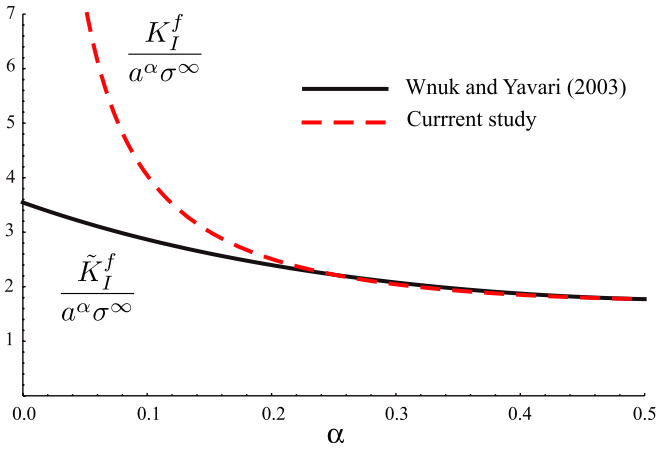

Figure 4. Comparison of fractal stress intensity factors from equations (46) and (41).

In this paper, we have directly calculated the stresses from a Westergaard stress function of a fractal crack with no approximations and arrived at expression (41). Let us briefly recall the steps taken by Wnuk and Yavari (2003) in the evaluation of FSIF. Assuming an even distribution of traction $p(x)$, i.e. $p(-x) = p(x)$, evaluation of the integral (43) results in

$$\hat{K}_{\mathrm{I}}^{\mathrm{f}} = \frac{1}{(\pi a)^\alpha} \int_0^a p(x) \frac{(a-x)^{2\alpha} + (a+x)^{2\alpha}}{(a^2 - x^2)^\alpha} \mathrm{d}x. \tag{44}$$

However, the dimension of $\hat{K}_{\mathrm{I}}^{\mathrm{f}}$ is not consistent with dimension of FSIF defined by (37). To resolve this inconsistency they defined a pre-factor $C(\alpha, a)$, which was obtained from a dimensional analysis and it reads

$$C(\alpha, a) = \left(\frac{a}{\sqrt{\pi}} \right)^{2\alpha - 1}. \tag{45}$$

Finally, multiplying (44) by (45) gives the following relation for the FSIF as presented in Wnuk and Yavari (2003):

$$\tilde{K}_{\mathrm{I}}^{\mathrm{f}} = \frac{a^{\alpha-1}}{\pi^{2\alpha - 1/2}} \int_0^a p(x) \frac{(a-x)^{2\alpha} + (a+x)^{2\alpha}}{(a^2 - x^2)^\alpha} \mathrm{d}x. \tag{46}$$

The normalized FSIF resulting from this expression is compared with the one defined by (41) in figure 4. In summary, the cause of the difference between the two expressions for the fractal stress intensity factors is that in Wnuk and Yavari (2003) an approximate expression was used for calculating the stress intensity factor (43), while in the present work we have calculated stresses directly from the Westergaard stress function. Interestingly, as mentioned earlier the two expressions of FSIF show excellent agreement within the physically acceptable range of roughness exponent.

4. Stability considerations for quasistatic cracks

In LEFM and the related generalizations of it there is only one point of instability defining the transition from a stationary to a catastrophically propagating crack. The criteria used to determine this instability point for brittle and quasi-brittle solids are well known and can be described as follows: (i) Griffith's energy criterion, resulting in the relation between a critical stress and the length of the pre-existing crack a of the form $\sigma_{\mathrm{critical}} \propto \frac{1}{\sqrt{a}}$. (ii) Irwin's criterion, according to which the stress intensity factor K at the onset of crack propagation is set equal to the fracture toughness: $K(\sigma, a, \text{geometry}) = K_{\mathrm{c}}$, or equivalently the crack driving force G is set equal to its critical value: $G(\sigma, a, \text{geometry}) = G_{\mathrm{c}}$. (iii) For nonlinearly elastic or ductile solids that obey Hencky–Ilyushin (deformation) theory of plasticity the Irwin energy release rate G should be replaced by Eshelby–Rice's J-integral: $J(\sigma, a, \text{geometry}) = J_{\mathrm{c}}$. (iv) For ductile materials Wells (1963) suggested a criterion based on the crack-tip opening (COD or δ) criterion, namely $\delta_c = \delta(\sigma, a, \text{geometry})$. This concept, if interpreted in the framework of the cohesive crack model, may be shown to be equivalent to Eshelby–Rice's criterion for the onset of fracture propagation.

It can be readily shown that for the brittle limit of material behaviour all the above four criteria reduce to Griffith's equation. In the late 1960s a new concept of a 'stable quasi-static' crack was introduced by McClintock (1958) and extensively studied by various researchers. According to these studies the critical point (onset of catastrophic crack propagation) is preceded by propagation of a quasi-static crack that slowly increases in length but remains in equilibrium with the applied external load. Therefore, at any instant during this pre-fracture phase of deformation process, the applied driving force, measured by K_{applied}, G_{applied} or J_{applied}, equal their respective material counterparts K_{material}, G_{material} or J_{material}. These material characteristics are no longer just single numbers but are certain functions of the crack length a. These functions represent material resistance to crack extension (or 'tearing' process) and are usually denoted by the index R. Thus, during the quasi-static crack growth process the following equalities are satisfied.

$$\begin{aligned} K(\sigma, a, \text{geometry}) &= K_R(a), \\ G(\sigma, a, \text{geometry}) &= G_R(a), \\ J(\sigma, a, \text{geometry}) &= J_R(a). \end{aligned} \tag{47}$$

The expressions on the right-hand sides of these equations describe the so-called material resistance curves or 'material signature' curves. Since both G and J can be expressed by the first derivatives of the potential energy of a cracked body and the external loadings, it is noted that one may utilize this fact to determine the transition from stable to unstable crack growth by enforcing equalities between the second derivatives, namely

$$\begin{aligned} -\frac{\partial^2 \Pi}{\partial \ell^2} &= \left. \frac{\partial G}{\partial \ell} \right|_{\text{constant stress (or fixed grips)}} = \frac{\mathrm{d}G_R(\ell)}{\mathrm{d}\ell}, \\ -\frac{\partial^2 \Pi}{\partial \ell^2} &= \left. \frac{\partial J}{\partial \ell} \right|_{\text{constant stress (or fixed grips)}} = \frac{\mathrm{d}J_R(\ell)}{\mathrm{d}\ell}. \end{aligned} \tag{48}$$

Here for a finite crack of length $\ell = 2a$. The boundary conditions imposed on the surfaces of the solid body are either 'constant stress' or 'fixed grips'. Conditions (47) are satisfied throughout the SCG phase. When both (47) and (48)

are satisfied simultaneously the process of SCG ends and the catastrophic propagation of fracture begins. The critical states so determined are characterized by the final effective fracture toughness attained during the slow crack growth process and by the final crack length. In this way the critical stress level can be determined. For ductile solids (or for very rough cracks) this σ_{critical} substantially exceeds the stress at the onset of crack propagation σ_{initial}. It will be shown that the σ_{critical} versus a curve, as defined in the classical studies of quasi-brittle fracture, undergoes a separation as it splits into two distinct curves. Therefore, instead of one curve (such as the final result of Griffith's theory) one obtains two curves; one serves as a lower bound of the critical stress (onset of stable growth) and the other one as an upper bound (onset of catastrophic fracture). Such a phenomenon is illustrated in figure 9 in the next section. Study of the effects of material ductility and roughness of the crack surfaces on the slow crack growth and the attainment of the terminal instability is the primary objective of this work.

To mathematically describe pre-fracture processes that involve quasi-static cracks we apply Wnuk's criterion of 'delta COD' derived from the concept of 'structured cohesive zone' associated with a moving crack (Wnuk 1972, 1974). Quasi-static crack extension process in ductile solids is somewhat analogous to the time-dependent fracture in visco-elastic solids (Wnuk 1974). For the purpose of stability considerations we view the propagating crack as a sequence of local instability states, while the terminal instability is considered as a global instability tantamount to the onset of the catastrophic fracture. It is noted that for brittle solids the phenomenon of stable crack extension disappears altogether; this can be determined by the initial slope of the R-curve. Positive slope means that the slow growth is possible, while negative slope signifies the absence of the slow crack growth process. This is the case of perfectly brittle fracture described by Griffith (1921). In order to determine the transition from stable to unstable crack extension, the $J_R(a)$ material resistance curve will be represented[7] by the length of the cohesive zone R shown as a function of the current crack length, $R(a)$. This curve will be described by a nonlinear differential equation, which in the limiting case of a smooth crack reduces to the Wnuk–Rice–Sorensen differential equation (Wnuk 1972, Rice and Sorensen 1978, Rice *et al* 1980).

5. Transition from stable to unstable propagation of a quasi-static fractal crack

Stability problems for a quasi-static smooth crack have been studied in the past by Wnuk and Knauss (1970), Wnuk (1972, 1974), Rice and Sorensen (1978), Rice (1968), Rice *et al* (1980) and Budiansky (1988). Wnuk and Budiansky used the 'final stretch' (or so-called 'delta COD') criterion governing the propagation of a quasi-static crack, proposed by Wnuk (1972), which is identical to the differential equation describing the material R-curve derived independently by Rice and Sorensen (1978) six years later in 1978 and by Rice *et al* (1980). Their derivation was based on the analysis of the Prandtl slip line field in a rigid-plastic solid body weakened by a slowly propagating crack.

5.1. Final stretch criterion

Wnuk's criterion is linked to a structured cohesive crack model equipped with a process zone of finite size Δ. According to this criterion it is not the COD, but an increment of the COD measured at the outer edge of the process zone associated with the propagating crack (labelled with name 'State 1' in figure 5). It is postulated that this increment, denoted by $\hat{u}$, remains constant throughout the stable phase of the continuing subcritical growth of the crack, see figure 5 for details. As the cohesive crack model relates the energy release rate, measured by the J-integral, to the COD measured at the physical tip of the cohesive (extended) crack, say δ_t (alternatively to the length of the cohesive zone R) we can write

$$J = S\delta_t = \frac{8S^2R}{\pi E'}, \tag{49}$$

where E' is Young's modulus adjusted for either plane stress or plane strain, while S denotes the constant cohesive stress or the yield point depending on the range of the considered material ductility.

It is possible to express the first and the second derivatives of the potential energy Π associated with a solid body weakened by a crack and subjected to external loading in terms of the $\text{COD}_{\text{cohesive}}$. It turns out that for a fractal crack the functional relation between the $\text{COD}_{\text{cohesive}}$ and the distance x_1 measured from the physical tip of the propagating quasi-static crack (see figures 5 and figure 16) is remarkably similar to the one obtained for the smooth crack, provided that Barenblatt's condition of small size of the cohesive zone relative to the crack length is satisfied. In fact, our calculations show that the $\text{COD}^{\text{f}}_{\text{cohesive}}$ is related to the smooth case by a pre-factor $\kappa(\alpha)$ and redefining the size of the cohesive zone ahead of a fractal crack (R^{f}) (see the appendix). The end result of the solution pertaining to the $\text{COD}^{\text{f}}_{\text{cohesive}}$ of a fractal crack obtained by an application of the Wnuk–Yavari model reads[8]

$$v^{\text{f}}(x_1, R^{\text{f}}) = \kappa(\alpha)\frac{4S}{\pi E'}\left[\sqrt{R^{\text{f}}(R^{\text{f}} - x_1)} - \frac{x_1}{2}\ln\left(\frac{\sqrt{R^{\text{f}}} + \sqrt{R^{\text{f}} - x_1}}{\sqrt{R^{\text{f}}} - \sqrt{R^{\text{f}} - x_1}}\right)\right]. \tag{50}$$

Here the symbol x_1 is used to denote the distance measured from the tip of the physical crack while the fractal constraint factor $\kappa(\alpha)$ is defined in (95) and the ratio of the length R^{f} associated with a fractal crack to the length R is defined in

[7] When working with the cohesive crack model—and only within the small-scale-yielding restrictions (when the Barenbaltt condition is satisfied, $R \ll a$) it turns out that there exists a direct proportionality between the $\text{COD}_{\text{cohesive}}$—$J$-integral and the length of the cohesive zone R. If the Barenblatt condition is not satisfied, this is no longer so simple. Instead one can provide certain nonlinear equations, which connect all the three entities J, R and δ. In this context, instead of J-integral one may focus on R, because they differ only by a multiplicative constant, i.e. $J = \frac{8S^2}{\pi E'}R$.

[8] For the details on the calculation of the $\text{COD}_{\text{cohesive}}$ see the appendix, where we have derived the expressions for COD for a fractal crack.

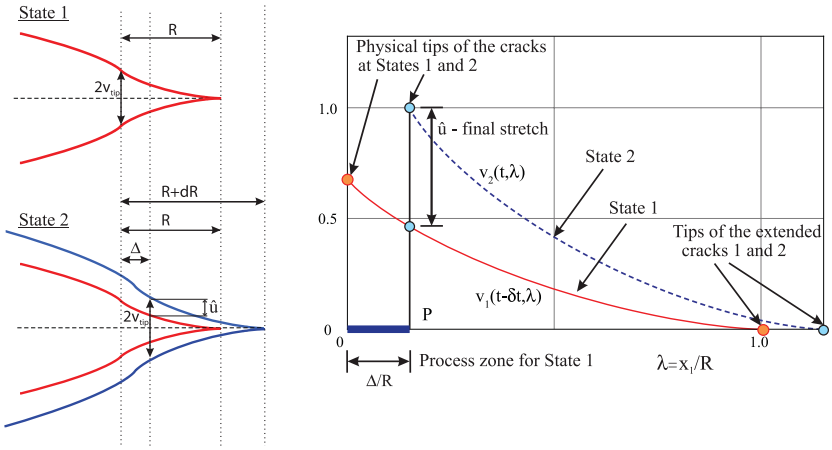

Figure 5. Distribution of the COD within the cohesive zone corresponding to two subsequent states in the course of quasi-static crack extension (Wnuk's criterion of delta COD).

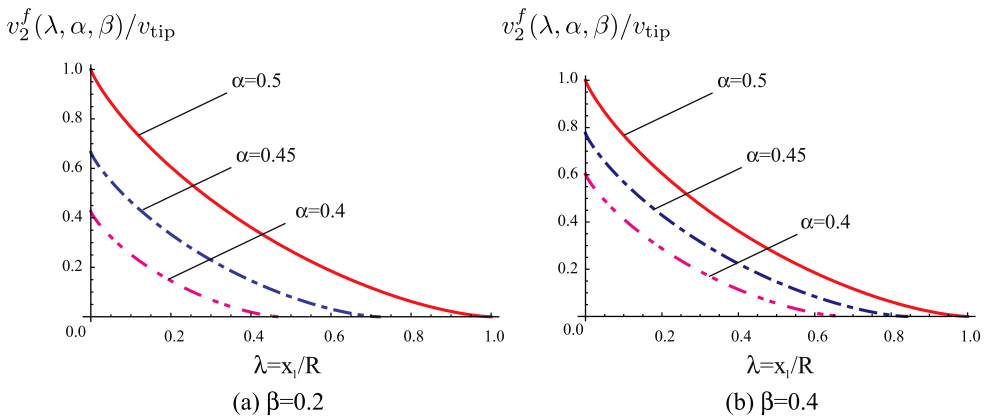

Figure 6. Distributions of the $\mathrm{COD}_{\mathrm{cohesive}}$ for smooth and rough cracks ($\alpha = 0.5$, 0.45 and 0.4) for (a) $\beta = 0.2$, (b) $\beta = 0.4$.

(89). Combining these equations results in

$$v^{\mathrm{f}}(x_1, R, \alpha, \beta) = \frac{4SN(\alpha,\beta)R}{\pi E'}\kappa(\alpha) \times\left[\sqrt{1-\frac{x_1}{N(\alpha,\beta)R}} -\frac{x_1}{2N(\alpha,\beta)R}\ln\left(\frac{1+\sqrt{1-\dfrac{x_1}{N(\alpha,\beta)R}}}{1-\sqrt{1-\dfrac{x_1}{N(\alpha,\beta)R}}}\right)\right], \tag{51}$$

or

$$v^{\mathrm{f}}(\lambda) = v^{\mathrm{f}}_{\mathrm{tip}}\left[\sqrt{1-\frac{\lambda}{N(\alpha,\beta)}} -\frac{\lambda}{2N(\alpha,\beta)}\ln\left(\frac{1+\sqrt{1-\dfrac{\lambda}{N(\alpha,\beta)}}}{1-\sqrt{1-\dfrac{\lambda}{N(\alpha,\beta)}}}\right)\right], \tag{52}$$

where

$$v^{\mathrm{f}}_{\mathrm{tip}} = N(\alpha,\beta)\kappa(\alpha)v_{\mathrm{tip}}, \qquad R^{\mathrm{f}} = N(\alpha,\beta)R, \qquad v_{\mathrm{tip}} = \frac{4SR}{\pi E'}. \tag{53}$$

Functions $N(\alpha, \beta)$ and $\kappa(\alpha)$ are defined in the appendix. Here the modulus $E' = E$ for plane stress and $E/(1-\nu^2)$ for plane strain, while x_1 has been replaced by a non-dimensional coordinate $\lambda = x_1/R$. The entity $v^{\mathrm{f}}_{\mathrm{tip}}$ represents half of the CTOD of a fractal crack, for which the degree of fractality is quantified by the exponent α and the ratio $\beta = \sigma/\sigma_{\mathrm{Y}}$. For any given set of (α, β) one may construct a plot of the opening displacement associated with a fractal crack, $\mathrm{COD}_{\mathrm{cohesive}}$. The plots of this kind are shown in figure 6. Note that each curve begins at a certain point on the vertical axis equal or less than one and ends at zero at the end of the extended crack (tantamount to the end of the cohesive zone). This means that the plots show the ratios $v^{\mathrm{f}}(\lambda)/v_{\mathrm{tip}}$. The differences between the curves shown in figure 6 appear significant, and we proceed to show that they lead to substantial differences in the stability properties of quasi-static rough cracks, as compared with a smooth crack. To substantiate this statement we shall now apply the delta COD criterion and determine the motion of the subcritical crack by establishing the governing equation for the J_R–Δa curve.

While brittle materials fracture at almost no irreversible strains, the ductile solids attain large strains prior to fracture. Ductility as a material property describes the ability of the material to undergo large irreversible strains before the onset of fracture. Following Hult and McClintock (1956) and Rice (1968), who defined 'ductility' in terms of the shear strains at the onset of yield (γ_Y) and at fracture (γ^f) in mode III fracture, and Wnuk and Mura (1981), who defined ductility for mode I fracture in terms of strains ϵ_Y and ϵ^f, we shall use the following definition of ductility:

$$\rho = \frac{R_{\text{initial}}}{\Delta} = \frac{\epsilon^f}{\epsilon_Y} = 1 + \frac{\epsilon^f_{\text{pl}}}{\epsilon_Y}. \tag{54}$$

Here ϵ^f_{pl} denotes the plastic component of the strain at fracture. It is noted that when $\rho \gg 1$ we deal with ductile materials, while for ρ approaching one we have the brittle limit of material behaviour. In the limit of $\rho = 1$, the entire nonlinear theory presented here reduces to the Griffith case, which exhibits no slow crack growth phenomenon.

5.2. Motion of a subcritical crack

Let us first recall that potential energy of a cracked linearly elastic solid is written as

$$\Pi(\sigma, \ell) = \frac{1}{2}\int_V \sigma_{ij}\varepsilon_{ij}\mathrm{d}V - \int_{S_T} T_i u_i \,\mathrm{d}S - SE(\ell). \tag{55}$$

J-integral is defined as

$$J = -\frac{\partial \Pi}{\partial \ell}. \tag{56}$$

Symbol $SE(\ell)$ in (55) denotes the surface energy due to a crack of length ℓ generated within a solid body. For a Griffith crack $\ell = 2a$. Replacing the J-integral by $2v_{\text{tip}}S$, where v_{tip} stands for the CTOD of the cohesive crack and S denotes the constant cohesive stress, we focus our attention on the crack-tip opening displacement $\text{COD}_{\text{cohesive}}$ expressed by (52). As it turns out, it is sufficient to use just the two quantities R and Δ and the two auxiliary functions $\kappa(\alpha)$ (93) and $N(\alpha, \beta)$ (89). These functions stem from the fractal geometry, which has been incorporated into the structured cohesive crack model. Here α is a measure of roughness of the crack surface and β is the stress ratio $\beta = \sigma/\sigma_Y$—alternatively—$\beta = \sigma/S$, if the magnitude of cohesive stress S rather than the yield point σ_Y is chosen to represent the constant restraining stress within the end-zone. The length characteristics involved in the representation of the opening displacement within the cohesive zone are R and Δ; the first denotes the equilibrium length of the cohesive zone and the latter describes the inner structure of the end-zone associated with a propagating quasi-static cohesive crack. Once the opening displacements within the cohesive zone are evaluated, one may proceed to apply the Wnuk's criterion of the final stretch governing the phenomenon of the continuing quasi-static crack motion.

$$[v_2^f(t - \delta t, 0) - v_1^f(t, \Delta)]_P = \hat{u}. \tag{57}$$

Here P denotes the control point shown in figure 5, while the constant $\hat{u}$ represents the 'final stretch', also shown in figure 5. Using (50) and expanding the function $R(x_1 = 0)$ into a Taylor series around the point $x_1 = \Delta$ the two functions v_2^f and v_1^f above are evaluated as follows:

$$\begin{aligned} v_2^f(P) &= v[0, R^f(0)] = \kappa(\alpha)\frac{4S}{\pi E'}R^f(0) \\ &= \kappa(\alpha)\frac{4S}{\pi E'}\left[R^f(\Delta) + \frac{\mathrm{d}R^f}{\mathrm{d}\ell}\Delta\right], \end{aligned} \tag{58}$$

$$\begin{aligned} v_1^f(P) &= v[\Delta, R^f(\Delta)] \\ &= \kappa(\alpha)\frac{4S}{\pi E'}\left[\sqrt{R^f(\Delta)[R^f(\Delta) - \Delta]}\right. \\ &\quad \left. - \frac{\Delta}{2}\ln\left(\frac{\sqrt{R^f(\Delta)} + \sqrt{R^f(\Delta) - \Delta}}{\sqrt{R^f(\Delta)} - \sqrt{R^f(\Delta) - \Delta}}\right)\right]. \end{aligned} \tag{59}$$

It is noted that for a moving crack both x_1 and R^f are time dependent, see figure 16. Using (58) and (59) we subtract v_1^f from v_2^f and apply the criterion (57) to obtain

$$\begin{aligned} &R^f + \Delta\frac{dR^f}{\mathrm{d}a} - \sqrt{R^f(R^f - \Delta)} \\ &\quad + \frac{\Delta}{2}\ln\left(\frac{\sqrt{R^f} + \sqrt{R^f - \Delta}}{\sqrt{R^f} - \sqrt{R^f - \Delta}}\right) = \hat{u}\frac{\pi E'}{4S\kappa(\alpha)}. \end{aligned} \tag{60}$$

Hence, a nonlinear ordinary differential equation follows:

$$\begin{aligned} \frac{\mathrm{d}R^f}{\mathrm{d}a} &= \frac{\hat{u}}{\Delta}\frac{\pi E'}{4S\kappa(\alpha)} - \frac{R^f}{\Delta} + \sqrt{\frac{R^f}{\Delta}\left(\frac{R^f}{\Delta} - 1\right)} \\ &\quad - \frac{1}{2}\ln\left(\frac{\sqrt{R^f} + \sqrt{R^f - \Delta}}{\sqrt{R^f} - \sqrt{R^f - \Delta}}\right). \end{aligned} \tag{61}$$

Denoting the group of material constants appearing as the first term on the right-hand side of (61) by the 'tearing modulus' M, and using (89) to relate R^f and R, we obtain

$$\begin{aligned} \frac{\mathrm{d}R}{\mathrm{d}a} &= \frac{1}{N(\alpha, \beta)}\left[M - \frac{N(\alpha, \beta)R}{\Delta}\right. \\ &\quad + \sqrt{\frac{N(\alpha, \beta)R}{\Delta}\left(\frac{N(\alpha, \beta)R}{\Delta} - 1\right)} \\ &\quad \left. - \frac{1}{2}\ln\left(\frac{\sqrt{\frac{N(\alpha, \beta)R}{\Delta}} + \sqrt{\frac{N(\alpha, \beta)R}{\Delta} - 1}}{\sqrt{\frac{N(\alpha, \beta)R}{\Delta}} - \sqrt{\frac{N(\alpha, \beta)R}{\Delta} - 1}}\right)\right]. \end{aligned} \tag{62}$$

The initial condition needed for integrating the ODE (62) is $R(a_0) = R_{\text{initial}}$, where $R_{\text{initial}} = (8/\pi)(K_c/S)^2$. The first term in the bracket on the right side of (62) represents the tearing modulus for the material, in which a rough quasi-static crack is propagating. The constant M is defined as

$$M = \frac{\hat{u}}{\Delta}\frac{\pi E'}{4S\kappa(\alpha)}. \tag{63}$$

We will show that this material constant strongly depends on material ductility $\rho = R_{\text{initial}}/\Delta$. We note that for a smooth crack the factor $\kappa(\alpha)$, and the ratio factor $N(\alpha, \beta)$ are both

equal to one, and (62) reverts to the Wnuk (1972) equation. The nonlinear ODE (62) can readily be solved numerically (see the appendix for details). We will use the following non-dimensional variables in the solution procedure of the nonlinear ODE:

$$\rho = \frac{R_{\text{initial}}}{\Delta}, \quad Y = \frac{R}{R_{\text{initial}}}, \quad X = \frac{a}{R_{\text{initial}}},$$
$$\frac{R^{\text{f}}}{\Delta} = \rho N(\alpha, \beta) Y, \tag{64}$$

where

$$N(\alpha, \beta) = 4\pi^{\frac{1}{2\alpha}-2}\left[\frac{\alpha\Gamma(\alpha)}{\Gamma(1/2+\alpha)}\right]^{\frac{1}{\alpha}} \beta^{1/\alpha-2}, \quad \beta = \frac{\sigma}{S}. \tag{65}$$

Using these non-dimensional variables, one can rewrite (62) in the following form

$$N(\alpha, \beta)\frac{\mathrm{d}Y}{\mathrm{d}X} = M - \rho N(\alpha, \beta) Y + \sqrt{\rho N(\alpha, \beta) Y\,[\rho N(\alpha, \beta) Y - 1]} - \frac{1}{2}\ln\left(\frac{\sqrt{\rho N(\alpha, \beta) Y} + \sqrt{\rho N(\alpha, \beta) Y - 1}}{\sqrt{\rho N(\alpha, \beta) Y} - \sqrt{\rho N(\alpha, \beta) Y - 1}}\right). \tag{66}$$

When the non-dimensional variables are used, the initial condition reads: $Y(X_0) = 1$. Equation (66) can be abbreviated as follows[9]

$$\frac{\mathrm{d}Y}{\mathrm{d}X} = F(Y, \rho, \alpha, \beta(X)), \tag{67}$$

where

$$F(Y, \rho, \alpha, \beta(X)) = \frac{1}{N(\alpha, \beta(X))}\left[M - \rho N(\alpha, \beta(X)) Y + \sqrt{\rho N(\alpha, \beta(X)) Y\,[\rho N(\alpha, \beta(X)) Y - 1]} - \frac{1}{2}\ln\left(\frac{\sqrt{\rho N(\alpha, \beta(X)) Y} + \sqrt{\rho N(\alpha, \beta(X)) Y - 1}}{\sqrt{\rho N(\alpha, \beta(X)) Y} - \sqrt{\rho N(\alpha, \beta(X)) Y - 1}}\right)\right]. \tag{68}$$

The next step is to find the solution of (67). Since it cannot be obtained in closed form we use Mathematica®. Solving this equation we obtain the unknown material resistance function $Y = Y(X)$. Interestingly, there exists a certain threshold for the tearing modulus M, referred to as M_{minimum}, below which the phenomenon of SCG is not possible. Parametric studies show that the influence of α on the minimum tearing modulus is negligible. Therefore, using $\alpha = 0.5$ and requiring the slope $\mathrm{d}Y/\mathrm{d}X$ in (67) to be positive, we obtain a relation between M_{minimum} and the ductility parameter ρ, namely

$$M_{\text{minimum}}(\rho) = \rho - \sqrt{\rho(\rho-1)} + \frac{1}{2}\ln\left(\frac{\sqrt{\rho} + \sqrt{\rho-1}}{\sqrt{\rho} - \sqrt{\rho-1}}\right). \tag{69}$$

In the calculations that follow we assume that the actual tearing modulus M is 10% higher than the minimum value determined by (69), i.e.[10]

$$M(\rho) = 1.1 M_{\text{minimum}}(\rho). \tag{70}$$

[9] During the subcritical growth of cracks β is a function of the crack nominal length X. For more details see the appendix.

[10] We simply assume that the tearing modulus is slightly higher than the minimum tearing modulus M_{minimum}, because without such an assumption there will be no SCG prior to catastrophic fracture.

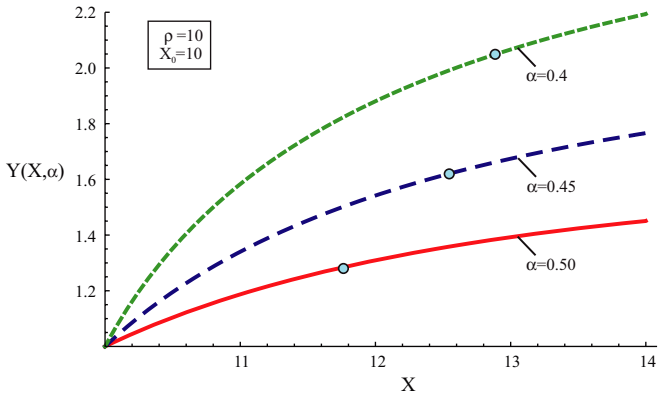

Figure 7. Material resistance curves obtained for $X_0 = 10$, ductility index $\rho = 10$, and three values of the fractal exponent $\alpha = 0.50$, 0.45 and 0.40. It should be noted that for the rougher crack surfaces the slope of the R-curve increases. The R-curves shown here depend on the material properties (such as ductility) and fractal geometry only, but the location of the terminal instability point is also influenced by geometrical configuration of a pre-cracked specimen. For the Griffith crack configuration the transition between stable and unstable crack growth is defined by two coordinates: crack length at fracture X_{f}, and material toughness at fracture Y_{f}. With the ductility index $\rho = 10$ and the initial crack length $X_0 = 10$ the terminal states were found to be: for $\alpha = 0.5$, $X_{\text{f}} = 11.764$ and $Y_{\text{f}} = 1.287$; for $\alpha = 0.45$, $X_{\text{f}} = 12.542$ and $Y_{\text{f}} = 1.620$; for $\alpha = 0.4$, $X_{\text{f}} = 12.862$ and $Y_{\text{f}} = 2.045$. These points are shown by little circles inserted in the graphs representing the R-curves.

Now by having $M(\rho)$ it is possible to solve (66). The details of the solution procedure are described in the appendix. We have plotted the solution of (66) in several different ways. In figure 7 the non-dimensional material resistance parameter $Y(X)$ is plotted as a function of crack nominal length for different values of roughness exponent when $\rho = 10$ and $X_0 = 10$. It is seen that the slope of the material resistance curve is higher for rougher cracks, so the material resistance to fracture for rougher cracks is higher. Further important information that can be extracted from the solution of (66) is the dependence of the external load on the current crack length developed during the phase of SCG. As we have shown in the appendix, during the SCG phase, the loading ratio $\beta = \sigma/S$ is a function of X. The resulting $\beta(X)$ curve is shown in figure 8. As can be seen in this figure the required applied loading for rougher cracks is higher than that of a smooth crack. Finally, in figure 9 we have shown the maximum and minimum values of β attained in the process of subcritical crack growth. These limits are important in the stability analysis, since for loadings exceeding β_{initial} the SCG takes place and when β reaches β_{maximum} the catastrophic failure begins. In figure 9 these parameters are shown as functions of X_0 and α. The plots show that for cracks with higher initial length X_0 the sustainable loading is lower, but it always exceeds the catastrophic load predicted for a smooth crack.

It is noted that the differential equation (66) can be considerably simplified for the limiting case $R \gg \Delta$, which corresponds to a more ductile behaviour of the material during the fracture process. When the right-hand side of (66) is expanded into a Taylor series and the terms of the order $O((\Delta/R)^2)$ are neglected, the following simplified form of

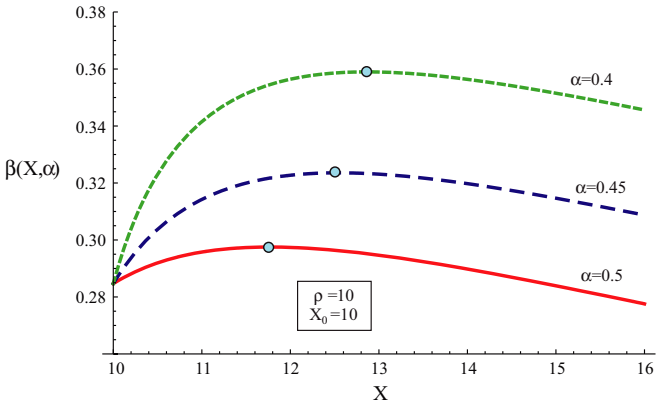

Figure 8. During SCG stage the non-dimensional loading ratio $\beta = \frac{\sigma}{S} = \frac{2}{\pi}\sqrt{\frac{2Y(X)}{X}}$ is a monotonically increasing function of either toughness (Y) or the current crack length (X) up to the critical point designated by the maximum on each curve. Maxima shown on the loading curves correspond to the terminal instability states. For the ductility index $\rho = 10$ and the initial crack length of $X_0 = 10$, the applied stress at the onset of crack growth is $\sigma_{\text{initial}} = 0.285S$. The critical stress σ_{critical} attained at the end of the slow crack growth process equals $0.297S$ when $\alpha = 0.5$, then 0.324 for $\alpha = 0.45$, and 0.359 for $\alpha = 0.40$. For $\alpha = 0.5$ we have 4.5% increase in the applied load, for $\alpha = 0.45$ this increase is 13.6%, and for $\alpha = 0.4$ it is 26.1%.

the governing equation is obtained:

$$\frac{\mathrm{d}R^{\mathrm{f}}}{\mathrm{d}a} = \overline{M}(\rho) - \frac{1}{2} - \frac{1}{2}\ln\left(\frac{4R^{\mathrm{f}}}{\Delta}\right). \tag{71}$$

Here the tearing modulus M is renamed as $\overline{M}(\rho)$ and is defined by the following expression:

$$\overline{M}(\rho) = 1.1[\tfrac{1}{2} + \tfrac{1}{2}\ln(4\rho)]. \tag{72}$$

Thus, (71) is rewritten in the following form

$$\frac{\mathrm{d}R}{\mathrm{d}a} = \frac{1}{N(\alpha, \beta(X))}\left[\overline{M}(\rho) - \frac{1}{2} - \frac{1}{2}\ln\left(\frac{4\rho N(\alpha, \beta(X))R}{\Delta}\right)\right]. \tag{73}$$

Non-dimensional governing ODE. Using the non-dimensional variables defined in (64), the differential equation (73) can be recast into a form containing only dimensionless quantities Y, X, ρ, α and β as

$$\frac{\mathrm{d}Y}{\mathrm{d}X} = \frac{1}{N(\alpha, \beta(X))}\left[\overline{M}(\rho) - \frac{1}{2} - \frac{1}{2}\ln\left[4\rho N(\alpha, \beta(X))Y\right]\right]. \tag{74}$$

Some further algebraic transformations allow one to reduce this equation to a form equivalent to the Wnuk–Rice–Sorensen equation describing motion of a stable quasi-static smooth crack. Rewriting (74), which is valid for a fractal crack, one obtains the following form for the governing differential equation:

$$\frac{\mathrm{d}Y}{\mathrm{d}X} = \frac{1}{2N(\alpha, \beta(X))}\ln\left[\frac{m(\rho, \alpha, \beta(X))}{Y}\right], \tag{75}$$

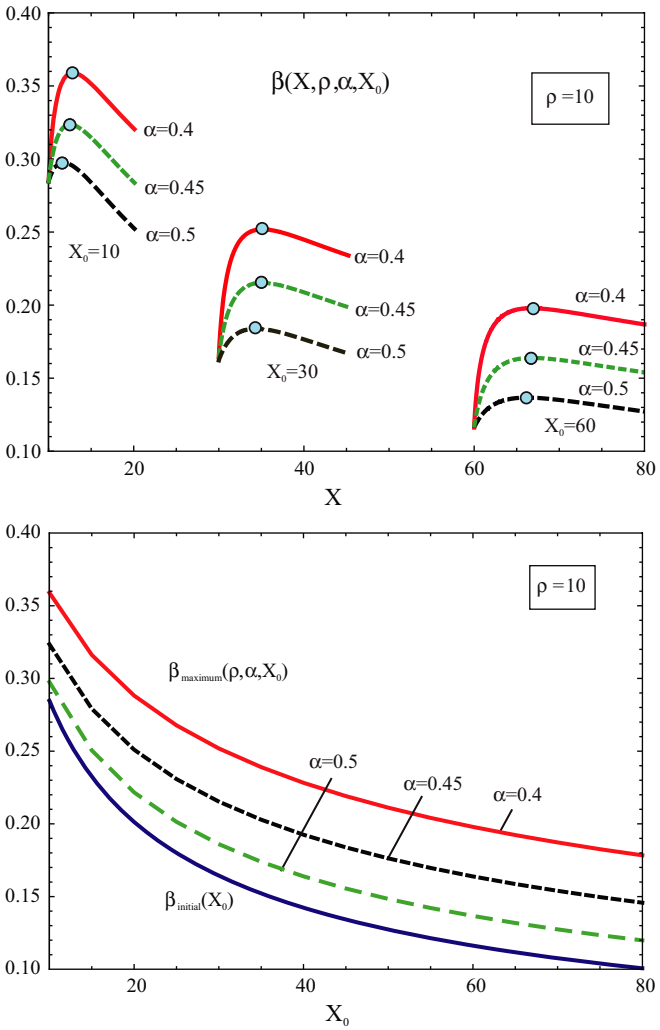

Figure 9. Top. Loading curves corresponding to three values of initial crack length ($X_0 = 10$, 30 and 60). Maxima shown on the loading curves correspond to the terminal instability states. Bottom. The loci of β_{initial} and β_{maximum} for different values of roughness exponent α and $\rho = 10$ shown as functions of X_0. Note that $\beta_{\text{initial}} = \frac{2}{\pi}\sqrt{\frac{2}{X_0}}$, while the tearing modulus $M = 1.1M_{\text{minimum}}$.

where

$$m(\rho, \alpha, \beta(X)) = \frac{\mathrm{e}^{2\overline{M}(\rho)-1}}{4\rho N(\alpha, \beta(X))}. \tag{76}$$

If the right-hand side of (74) is denoted by $\mathrm{RF}(Y, \rho, \alpha, \beta(X))$, the governing differential equation (74) reads $\mathrm{d}Y/\mathrm{d}X = \mathrm{RF}(Y, \rho, \alpha, \beta(X))$. The function RF defines the slope of the R-curve and is illustrated in figure 10 (bottom). Note that RF for $\rho \gg 1$ very closely approximates the function $F(Y, \rho, \alpha, \beta(X))$ defined in (67) and valid for an arbitrary value of the ductility index ρ.

Note that for a smooth crack the ratio factor $N(0.5, \beta) = 1$ and thus the expressions in (75) and (76) reduce to the Wnuk–Rice–Sorensen equation describing the material R-curve that results from considerations of the stable crack extension phenomenon for a smooth crack. Here the function $m(\rho, \alpha, \beta(X))$ is a measure of the ratio of the steady-state length of the cohesive zone attained as an asymptotic value of an uninterrupted SCG, $R_{\text{steady state}}$ to the threshold value of R,

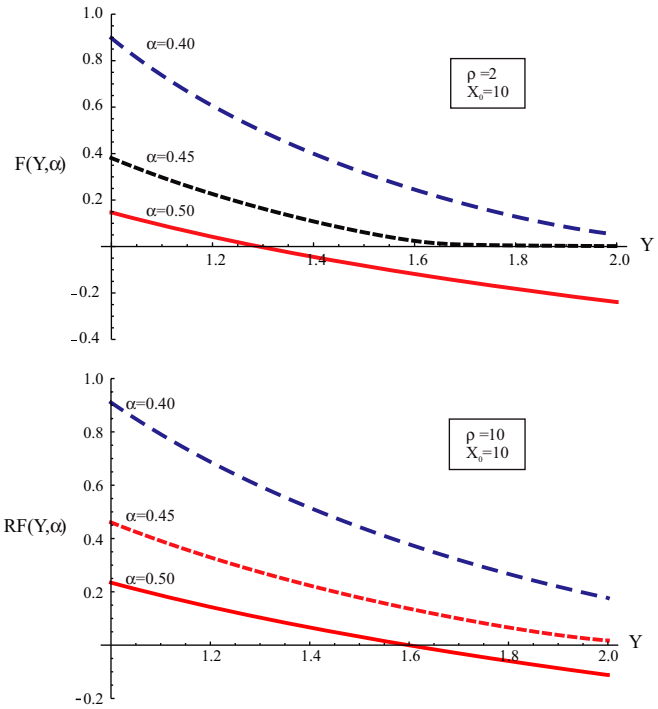

Figure 10. Top. Slopes of the material resistance curves associated with smooth crack (the lowest curve) and rough cracks. Higher slope of the R-curve signifies more pronounced subcritical crack propagation leading to higher values of the effective toughness and the critical crack length attained at the end of SCG phase. Value of the function F at $Y = 1$ denotes the initial slope of the R-curve and in engineering applications it is used as a measure of 'tearing resistance' of the material. For all the three curves shown the initial crack length is $X_0 = 10$, while the ductility index is $\rho = 2$. When these slopes are negative, SCG is not possible. Bottom: Slopes of the J_R (or just R) material resistance curves shown as functions of the effective toughness, which reflects enhancement of the initial toughness due to the process of slow crack extension, shown for $\rho = 10$ and three different values of the roughness parameter α.

labelled R_{initial}. In fact, for the smooth crack, when $\alpha = 0.5$ and $\kappa = 1$, the formulae given in (75) and (76) degenerate into the simple form given by Wnuk (1972, 1974) and valid for a smooth crack, namely

$$\frac{\mathrm{d}Y}{\mathrm{d}X} = \frac{1}{2}\ln\left[\frac{n(\rho)}{Y}\right], \qquad n(\rho) = \frac{R_{\text{steady state}}}{R_{\text{initial}}} = \frac{1}{4\rho}\mathrm{e}^{2\overline{M}(\rho)-1}. \tag{77}$$

The presence of roughness not only leads to a higher effective material toughness, but it also raises the critical nominal crack length and the critical stress attained at the end of the slow crack growth process. Another suitable parameter useful for estimating material resistance to subcritical crack propagation is the initial slope of the R-curve, namely

$$\left.\frac{\mathrm{d}Y}{\mathrm{d}X}\right|_{\text{initial}}^{\text{fractal}} = \frac{1}{N(\alpha,\beta(X_0))} \times\left\{\overline{M}(\rho) - \frac{1}{2} - \frac{1}{2}\ln\left[4\rho N(\alpha,\beta(X_0))\right]\right\} = \frac{1}{2N(\alpha,\beta(X_0))}\ln\left[m(\rho,\alpha,\beta(X_0))\right]. \tag{78}$$

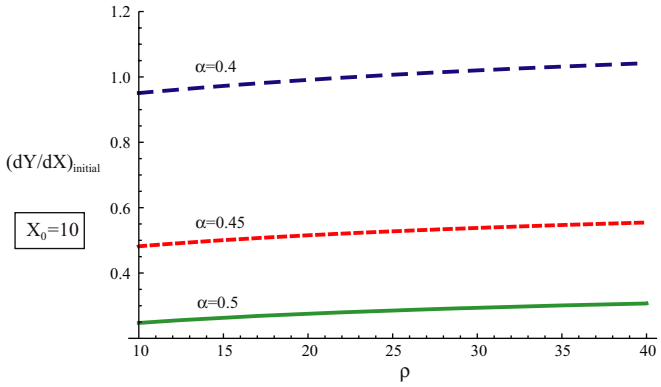

Figure 11. The initial slopes of the R-curve for different values of roughness index α as a function of ductility index ρ.

And

$$\left.\frac{\mathrm{d}Y}{\mathrm{d}X}\right|_{\text{initial}}^{\text{smooth}} = \overline{M}(\rho) - \frac{1}{2} - \frac{1}{2}\ln(4\rho) = \frac{1}{2}\ln\left[n(\rho)\right]. \tag{79}$$

The initial slope (78) is plotted in figure 11 for different values of α. These plots demonstrate that the initial slope $(\mathrm{d}Y/\mathrm{d}X)_{\text{initial}}$ is somewhat higher for a fractal crack, and this suggests another observation of physical significance: A body containing a fractal crack provides a higher effective resistance against crack propagation.

Paris *et al* (1977) and Hutchinson and Paris (1977) have connected the tearing modulus T_J present in the differential equation defining a material R-curve in terms of $J_R = J_R(a)$, to the initial slope of the J_R curve, $(\mathrm{d}J_R/\mathrm{d}a)_{\text{initial}}$, as follows:

$$T_J = \frac{E'}{\sigma_{\mathrm{Y}}^2}\left(\frac{\mathrm{d}J_R}{\mathrm{d}a}\right)_{\text{initial}} = \frac{\pi}{8}\left(\frac{\mathrm{d}R}{\mathrm{d}a}\right)_{\text{initial}}. \tag{80}$$

It is easily seen from figure 11 that an increase in the material ductility and/or the degree of fractality (roughness of the crack surface) substantially enhances the tearing modulus. Physically it means appearance of a more pronounced SCG and the ensuing reduction of the danger of the catastrophic fracture. The parameter T_J is used in the design for residual strength in pressure vessels and other high reliability components used in nuclear power plants based on the R-curve approach.

6. Terminal instability state

Finding the coordinates $(X_{\mathrm{f}}, Y_{\mathrm{f}})$ characterizing the terminal instability state is of great importance in the stability analysis. Because of the complexity of the governing differential equations for the fractal crack problems it is necessary to find these points by numerical methods. We have described the method of solution in detail in the last part of the appendix. The method of finding the terminal instability state for two different ductile materials is shown graphically in figure 12. The terminal instability states can be found from the intersection points between two sets of curves. The first curve, which is denoted by F (RF for high material ductility), stands for the slope of the material resistance curve and is determined either from (68) or (74) depending on the problem, while the second curve, which is denoted by FAP (RAP for high ductility

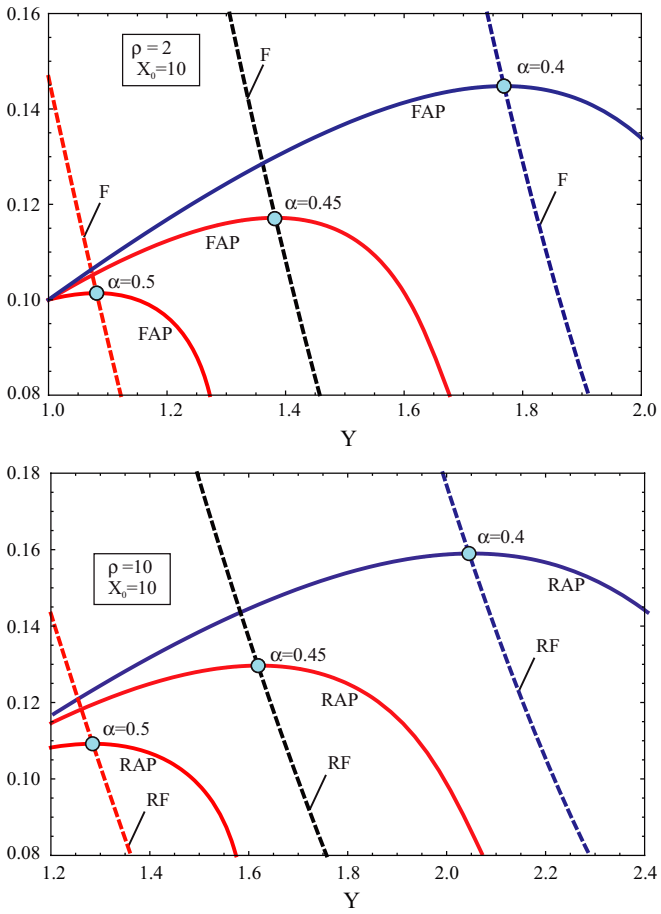

Figure 12. The intersection points of the two sets of curves (top)(F,FAP) and (bottom)(RF,RAP) define the terminal instability states, see equation (81). The F and RF functions represent the material resistance curve slope ($\mathrm{d}Y/\mathrm{d}X$) (see (68) and (74)) while FAP and RAP have been used for the determination of $\mathrm{d}Y/\mathrm{d}X$ resulted from applied loading (see (101)). Each critical state is determined by the final effective material toughness (Y_f) and the critical crack length (X_f). The curves shown are obtained for the initial crack length $X_0 = 10$ and three values of the roughness index α, and the ductility parameter $\rho = 2$ (top) and $\rho = 10$ (bottom). Tearing modulus M is assumed to be 10% higher than M_{minimum}.

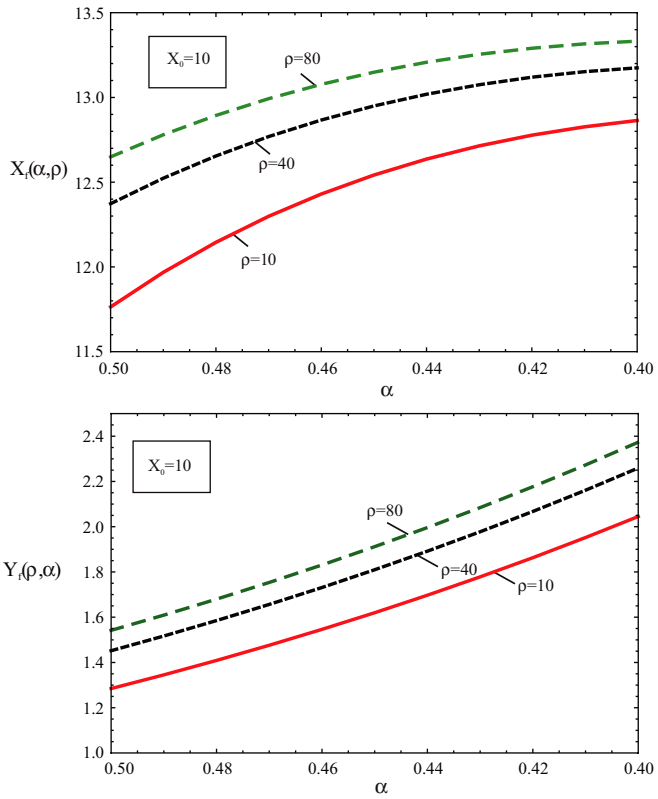

Figure 13. Coordinates of the terminal instability point (X_f, Y_f) shown as functions of fractal roughness parameter α. Top: critical crack length attained at the end of SCG phase. Bottom: effective material toughness attained at the end of SCG phase.

indices) and stands for the partial derivative of the applied energy release rate indicated by (99) and (100). Note that an almost linear relation between $\mathrm{d}Y/\mathrm{d}X$ and Y seen in figure 12 was confirmed experimentally for ductile grades of steel by Michel (1991).

Using the described procedure, we have plotted the results predicting the coordinates of the terminal instability states (X_f, Y_f) as functions of roughness index α (figure 13), material ductility ρ (figure 14), initial crack length X_0 (figure 15) and the stress ratio β. It is also worth noting that while for the quasi-brittle and brittle materials (for which Δ and R are of the same order of magnitude, i.e. $R \sim \Delta$) the extent of the SCG and the characteristics of the terminal instability point are described by the governing equation (67). A more frequently encountered case in materials engineering, for which Barenblatt's condition $R \gg \Delta$ holds, can be described by the simplified equations (74) or (75). Comparison of the results from the numerical solutions of (67) and (75) obtained at various values of parameters ρ, α and β shows that for a large material ductility index ρ (say $\rho > 6$) the difference between the results of the two formulae becomes negligible. At this point it is noted that the following four variables: (i) material ductility, $\rho = R_{\mathrm{initial}}/\Delta$, (ii) roughness measure of the crack surface, $\alpha = (2 - D)/2$ or $\alpha = (2H - 1)/2H$, where $1 < D < 2$ and $\frac{1}{2} < H < 1$, (iii) ratio of applied stress to the yield stress $\beta = \sigma/\sigma_\mathrm{Y}$ and (iv) initial size of the crack-like defect, $X_0 = a_0/R_{\mathrm{initial}}$ have a pronounced effect on the slope of the material resistance curve J_R–Δa and on the ensuing characteristics determining the terminal instability point, defined as the apparent toughness measure by J_R^{fracture} (or just R_{fracture} or the non-dimensional equivalent entity Y_f) and the critical nominal crack length a_{fracture} (or the non-dimensional X_f).

The trends observed in these studies of the slope of the material J_R–Δa curves are consistent with the physical phenomena studied experimentally and described in a recent paper by Alves *et al* (2010). These authors have shown that the slopes of the J_R–Δa curves obtained via an energy approach significantly increase when the roughness of the crack surface is accounted for. We obtain a similar result in the present work. In addition to this observation, it is shown that there exist substantial effects due to the initial crack size and due to the material ductility ($R_{\mathrm{initial}}/\Delta$). Introduction of Δ (process zone size in the context of this work) allows one to extend the results of the previous works into the domain of discrete (or quantized) fracture mechanics, say QFM, as suggested by

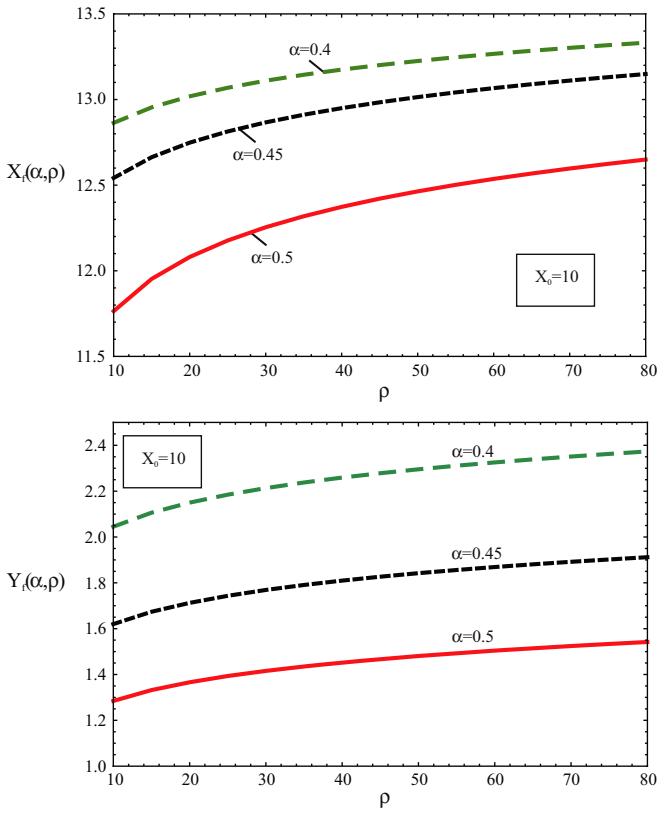

Figure 14. Coordinates of the terminal instability point (X_f, Y_f) shown as functions of material ductility. Top: critical crack length attained at the end of SCG phase. Bottom: effective material toughness attained at the end of SCG phase.

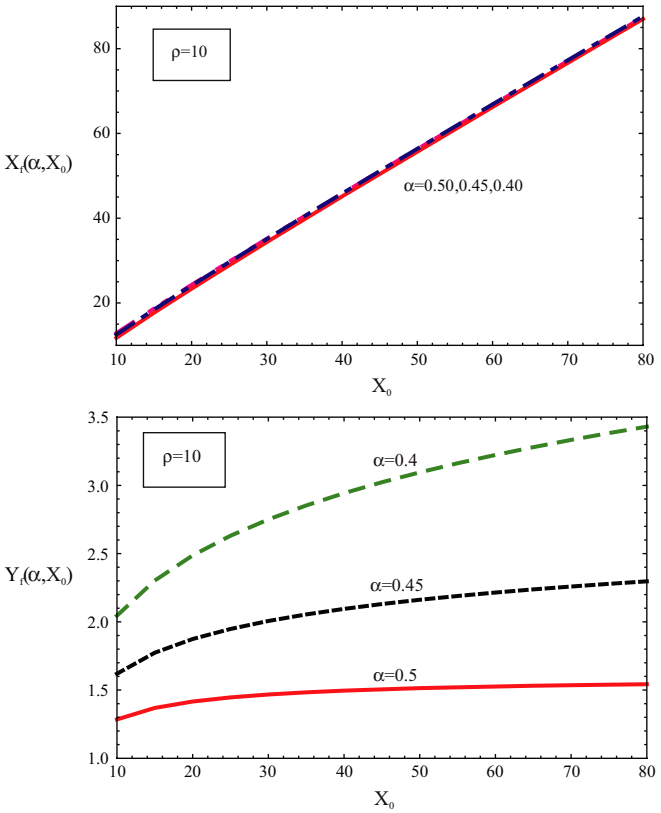

Figure 15. Coordinates of the terminal instability point (X_f, Y_f) shown as functions of initial crack length. Top: critical crack length attained at the end of SCG phase. Bottom: effective material toughness attained at the end of SCG phase.

Pugno and Ruoff (2004), Taylor *et al* (2005), and also by Wnuk and Yavari (2009). It is only for certain ranges of the pertinent variables such ρ, α and X_0 that the effects we describe here are visible. These effects are of particular importance in the nano-range of the pre-existing crack sizes. Similar observations can be made regarding the effects due to the material ductility and the roughness parameter on the characteristics of the terminal instability point. Interestingly, the minute variations in the latter result in large alterations of the final value of the material toughness and the critical crack length attained at the end of the slow SCG process. These preliminary findings encourage further studies of failure instability problems exploring the QFM representation of fracture process.

During the process of the stable growth of a quasi-static crack the rate of energy supply is always equal to the rate of energy demand. This kind of equilibrium between the two rates ensures the stability of the subcritical crack. However, at the end of this stable growth phase, when the transition to an unstable propagation occurs, it is necessary to use two conditions involving the rates of the energy supply and energy demand that must be simultaneously satisfied, namely

$$J(\ell, \sigma, \text{geometry}) = J_R(\ell),$$
$$-\frac{\partial^2 \Pi}{\partial \ell^2} = \left.\frac{\partial J}{\partial \ell}\right|_{\text{constant stress (or fixed grips)}} = \frac{\mathrm{d}J_R(\ell)}{\mathrm{d}\ell}. \qquad (81)$$

Geometrical interpretation of these two equations consists in a requirement that the crack driving force J–ℓ curve touches tangentially the material resistance curve $J_R(\ell)$. Calculations underlying the design of machine elements involving the residual strength concepts are made much less cumbersome if the terminal instability point is determined as the point of intersection between the curves independently representing the left-hand sides and the right-hand sides of the expressions given in (81) as functions of either X or Y, cf the graphs in figure 12. The graphs shown in these figures may be constructed only after the governing differential equation is solved for $Y = Y(X)$ revealing the function that determines the material resistance curve. Using this approach one may evaluate the coordinates of the respective intersection points, which represent the critical states. The coordinates of a critical state are: effective material toughness Y_f, final crack length X_f and the critical load σ_{critical}—all of them attained at the end of the pre-fracture slow crack extension process, figures 7, 8 and 9.

7. Conclusions

First, the stress functions for different fractal crack problems are presented with the help of the approximate Green's functions. These Green's functions are useful in the analytical treatment of bodies with fractal cracks. Next, using these stress functions the complete (and not asymptotic) expressions for the stress and strain fields around fractal cracks are obtained. Also Green's functions needed for the evaluation of the fractal stress

intensity factors (FSIF) in general cases are given. Then, these functions are utilized in the classical *final stretch criterion* of Wnuk (1972, 1974) applied to fractal cracks. In summarizing the essential results of the present work on the stability analysis the following two differential equations may be recalled:

$$\frac{dY}{dX} = F(Y(X), \rho, \alpha, \beta(X)) \qquad \text{(arbitrary } \rho\text{)}, \tag{82}$$

$$\frac{dY}{dX} = RF(Y(X), \rho, \alpha, \beta(X)) \qquad (\rho \gg 1). \tag{83}$$

These are two forms of the governing nonlinear ODE defining the material resistance curve in a ductile solid weakened by a propagating rough subcritical crack when described by a self-affine fractal curve. They reduce to the well-known equations of the smooth case $\alpha = 0.5$. The factor $m(\rho, \alpha, \beta)$, which is defined in (76), can be interpreted as the ratio of the material toughness developed at the steady state level, say $R_{\text{steady state}}$, to R_{initial}—the toughness measured by the length of the cohesive zone present at the onset of crack growth when $K = K_c$. It is noted that while (82) is valid for arbitrary values of the ductility index ρ (this includes the limiting case of brittle fracture when $\rho \to 1$), (83) holds for ductile materials for which $\rho \gg 1$. All the results obtained in this study are subject to the restriction imposed by the Barenblatt condition, $R \ll a$. We have demonstrated that the material ductility and/or roughness of the crack surfaces have a significant influence on enhancement of the characteristics pertinent to the terminal instability state. This influence becomes even more pronounced for very short cracks that compare in size with the characteristic length of the material; R_{initial} at the meso-level and Δ for the nano-level. It is noteworthy that while for ductile solids these two material length characteristics differ significantly, they converge to a common value in the limit of a perfectly brittle material. In the limiting case of perfectly brittle fracture both Δ and R_{initial} acquire the sense of the quantum fracture a_0 (Wnuk and Yavari 2009). Higher values of the critical crack length attained at the end of the slow crack growth process (X_f) are related to larger equilibrium cohesive zones ensuing at the terminal instability state. The lengths (R_{fracture} or Y_f) are used in our model as the measure of the effective material toughness developed during the pre-fracture crack extension process is clearly seen in figure 7 and in figures 12, 13, 14 and 15. These conclusions are entirely consistent with the findings of Wnuk and Yavari (2009).

As was mentioned earlier, analysis of (82) and (83) gives valuable information on the contribution of the parameters pertinent in the subcritical crack growth studies. These parameters and their effects are briefly recalled here as follows:

(i) Roughness measure of the crack surface, $\alpha = (2-D)/2$ or $\alpha = (2H-1)/2H$, where $1 < D < 2$ and $\frac{1}{2} < H < 1$: our analysis shows that the slope of material resistance curve for rougher cracks is higher. Consequently, the loading at which catastrophic failure occurs σ_{maximum} will be higher for rougher cracks. Roughness of the cracks also affects the critical crack length X_f. As is seen in figures 13 and 14, rougher cracks lead to larger critical lengths.

(ii) Material ductility, $\rho = R_{\text{initial}}/\Delta$: material ductility has a significant effect on the resistance of a cracked solid to fracture propagation. As expected the terminal instability point is higher for materials with higher ductility.

(iii) Initial nominal crack length, X_0: increasing the initial size of the crack leads to a decrease in the stress at fracture onset in a manner similar to the case of Griffith's crack.

Appendix. Auxiliary expressions needed for stability analysis of fractal cracks

In this appendix we derive some expressions that are needed for the stability analysis of fractal cracks. It should be noted that our stability analysis is based on the assumption of small-scale yielding, which corresponds to $R \ll a$, where R is the length of the yield zone ahead of the crack. First we determine the length of the cohesive zone ahead of a fractal crack (R^f). The size of the cohesive zone can be determined by enforcing the following finiteness condition at the crack tip:

$$K_I^{f(\text{applied})} + K_I^{f(\text{cohesive})} = 0. \tag{84}$$

From (33) the cohesive fractal stress intensity factor is calculated as

$$K_I^{f(\text{cohesive})} = -\frac{2^\alpha S \left(R^f\right)^\alpha}{\alpha \pi^{1-\alpha}}. \tag{85}$$

A.1. Size of the fractal yield zone

The applied fractal stress intensity factor (FSIF) depending on the problem can be calculated from either (32) or (39)[11]. Now by the use of (84) the length of the plastic zone ahead of the fractal crack (R^f) is obtained as

$$R^f = \frac{(\alpha\pi^{1-\alpha})^{1/\alpha}}{2}\left[\frac{K_I^{f(\text{applied})}}{S}\right]^{1/\alpha}. \tag{86}$$

The expressions for R and R^f are given in table 1. Thus, R^f/R reads

$$\frac{R^f}{R} = \frac{\dfrac{(\alpha\pi^{1-\alpha})^{1/\alpha}}{2}\left[\dfrac{K_I^{f(\text{applied})}}{S}\right]^{1/\alpha}}{\dfrac{\pi}{8}\left(\dfrac{K_I^{\text{applied}}}{S}\right)^2}. \tag{87}$$

[11] A couple of remarks are in order. We assume small-scale yielding because the size of the yield zone is very small compared with the nominal size of the crack half-length (a). This means that we should use the semi-infinite crack stress intensity factor formula to determine $K_I^{f(\text{cohesive})}$ and $K_I^{f(\text{applied})}$. If load is applied in the close vicinity of the crack tip and the length of the loaded zone is small compared with a, using the semi-infinite crack formula (32) is adequate. However, if load is applied along large segment(s) of the crack or at points distant from the crack tip, the finite crack solution for fractal stress intensity factor (39) is required.

Table 1. Required functions and expressions for strip yield model in both smooth and fractal crack cases.

Smooth case	Fractal case
$Z_{\text{applied}} = \dfrac{K_{\text{I}}^{\text{applied}}}{\sqrt{2\pi\zeta}}$	$Z^{\text{f}}_{\text{applied}} = \dfrac{1}{e^{i(\frac{1}{2}-\alpha)\theta}} \dfrac{K_{\text{I}}^{\text{f(applied)}}}{(2\pi\zeta)^{\alpha}}$
$Z_{\text{cohesive}} = -\dfrac{2S}{\pi}\left(\sqrt{\dfrac{R}{\zeta}} - \tan^{-1}\sqrt{\dfrac{R}{\zeta}}\right)$	$Z^{\text{f}}_{\text{cohesive}} = -\dfrac{S}{\pi(1+\alpha)} \dfrac{1}{e^{i(\frac{1}{2}-\alpha)\theta}} \left(\dfrac{R^{\text{f}}}{\zeta}\right)^{1+\alpha} f\left(1+\alpha, 1, 2+\alpha; -\dfrac{R^{\text{f}}}{\zeta}\right)$
$R = \dfrac{\pi}{8}\left(\dfrac{K_{\text{I}}^{\text{applied}}}{S}\right)^2$	$R^{\text{f}} = \dfrac{(\alpha\pi^{1-\alpha})^{1/\alpha}}{2}\left(\dfrac{K_{\text{I}}^{\text{f(applied)}}}{S}\right)^{1/\alpha}$
$v_{\text{crack}} = \dfrac{2S}{\pi E'}(4\sqrt{R\lvert\xi\rvert})$	$v^{\text{f}}_{\text{crack}} = \dfrac{2S}{\pi E'}\left(\dfrac{(R^{\text{f}})^{\alpha}\lvert\xi\rvert^{1-\alpha}}{\alpha(1-\alpha)}\right) = \dfrac{2S}{\pi E'}\left(\dfrac{R^{\text{f}}}{\alpha(1-\alpha)}\left(\dfrac{\lvert\xi\rvert}{R^{\text{f}}}\right)^{1-\alpha}\right)$
$v_{\text{cohesive}} = \dfrac{2S}{\pi E'}\left(2\sqrt{R\lvert\xi\rvert} + (R+\xi)\ln\left\lvert\dfrac{\sqrt{\lvert\xi\rvert}+\sqrt{R}}{\sqrt{\lvert\xi\rvert}-\sqrt{R}}\right\rvert\right)$	$v^{\text{f}}_{\text{cohesive}} = \dfrac{2S}{\pi E'}\text{Im}\left(\dfrac{R^{\text{f}}}{\alpha(1+\alpha)}\left(\dfrac{R^{\text{f}}}{\xi}\right)^{\alpha} f\left(1, \alpha, 2+\alpha; \dfrac{-R^{\text{f}}}{\xi}\right)\right)$

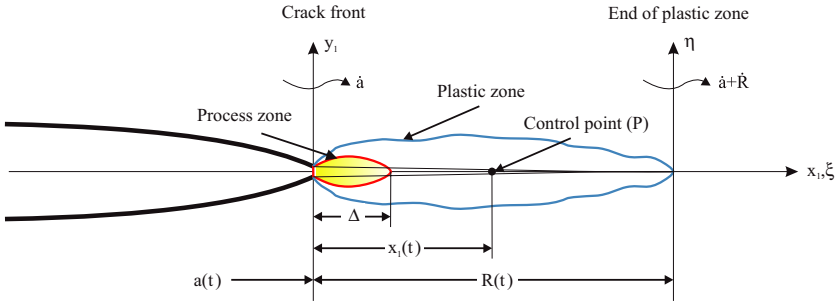

Figure 16. Front of an advancing crack and the associated yield (or crazed) zone.

This ratio can be simplified using (39)[12] to read

$$\frac{R^{\text{f}}}{R} = 4\alpha^{1/\alpha} S^{2-1/\alpha} \frac{\left(\int_0^1 \dfrac{2p(t)}{(1-t^2)^{1-\alpha}}\,\text{d}t\right)^{1/\alpha}}{\left(\int_0^1 \dfrac{2p(t)}{\sqrt{1-t^2}}\,\text{d}t\right)^2}. \tag{88}$$

As is seen R^{f}/R depends not only on α but also on S and $p(x)$. For uniform pressure distribution $p(x) = \sigma$ this ratio is simplified as follows:

$$\frac{R^{\text{f}}}{R} = N(\alpha, \beta), \tag{89}$$

where $\beta = \frac{\sigma}{S}$ and

$$N(\alpha, \beta) = 4\pi^{\frac{1}{2\alpha}-2}\left[\frac{\alpha\Gamma(\alpha)}{\Gamma(1/2+\alpha)}\right]^{\frac{1}{\alpha}} \beta^{1/\alpha-2}. \tag{90}$$

Γ stands for the Gamma function, while $N(\alpha, \beta)$ is referred to as the 'ratio factor'.

[12] Note that

$$\begin{aligned} K_{\text{I}}^{\text{f}} &= \left(\frac{a}{\pi}\right)^{1-\alpha}\int_0^a \frac{2p(x)}{(a^2-x^2)^{1-\alpha}}\text{d}x \\ &= \left(\frac{a}{\pi}\right)^{1-\alpha}\int_0^1 \frac{2p(t)}{a^{2-2\alpha}(1-t^2)^{1-\alpha}}a\,\text{d}t \\ &= \frac{a^{\alpha}}{\pi^{1-\alpha}}\int_0^1 \frac{2p(t)}{(1-t^2)^{1-\alpha}}\text{d}t, \end{aligned}$$

where $t = x/a$.

A.2. Fractal COD

After finding the length of the cohesive zone ahead of a fractal crack, it is required to derive the expression representing the COD within the cohesive zone. In table 1 the basic expressions required for determination of the COD within the cohesive zone are gathered. Vertical displacements (v or v^{f} for the fractal case)[13] inside the cohesive zone can be calculated using table 1 for both smooth and fractal cases. The results are as follows:

Smooth case. (Barenblatt 1962, Irwin *et al* 1969)

$$v_{\text{total}} = \frac{2S}{\pi E'}\left(2\sqrt{R\lvert\xi\rvert} - (R+\xi)\ln\left\lvert\frac{\sqrt{\lvert\xi\rvert}+\sqrt{R}}{\sqrt{\lvert\xi\rvert}-\sqrt{R}}\right\rvert\right) \quad \xi < 0, \tag{91}$$

where ξ is the coordinate of a point inside the cohesive zone (at the tip of the cohesive crack $\xi = 0$ and at the tip of the physical crack $\xi = -R$), i.e. $|\xi| = R - x_1$ (see figure 16).

Fractal case.

$$v^{\text{f}}_{\text{total}} = \frac{2S}{\pi E'}\left\{\frac{R^{\text{f}}}{\alpha(1-\alpha)}\left(\frac{\lvert\xi\rvert}{R^{\text{f}}}\right)^{1-\alpha} - \text{Im}\left[\frac{R^{\text{f}}}{\alpha(1+\alpha)}\left(\frac{R^{\text{f}}}{\xi}\right)^{\alpha} f\left(1, \alpha, 2+\alpha; -\frac{R^{\text{f}}}{\xi}\right)\right]\right\}, \quad \xi < 0, \tag{92}$$

[13] Note that COD is related to the vertical displacement by COD $= 2v$.

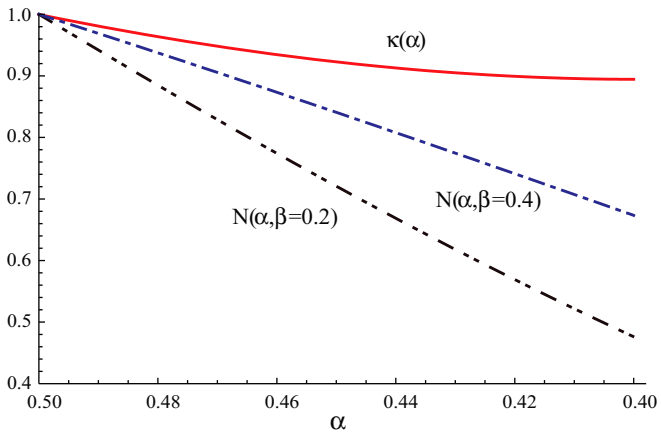

Figure 17. Graphs of the fractal constraint factor $\kappa(\alpha)$, and the ratio factor $N(\alpha, \beta)$ for $\beta = 0.2, 0.4$ for different values of roughness index. Functions $\kappa(\alpha)$ and $N(\alpha, \beta)$ appear in the expressions for the opening displacement within the cohesive zone associated with a fractal crack.

where the function f was defined in (28). The expression for $v^{\mathrm{f}}_{\mathrm{total}}$ is not in the form of elementary functions, so we have determined its values using Mathematica®. Interestingly, our calculations show that for moderately rough cracks the fractal vertical displacement (v^{f}) can be related to the classic result for a smooth crack v as shown in (52). For conversion of the smooth crack result (91) into the fractal crack case two functions are needed: $\kappa(\alpha)$ and $N(\alpha, \beta)$ (see (90)). Denoting

$$\kappa(\alpha) = \frac{v^{\mathrm{f}}_{\mathrm{tip}}}{v_{\mathrm{tip}}} \frac{R}{R^{\mathrm{f}}}, \tag{93}$$

$v^{\mathrm{f}}_{\mathrm{total}}$ is now written as

$$v^{\mathrm{f}}_{\mathrm{total}} = \kappa(\alpha) \frac{4S}{\pi E'} \left\{ \sqrt{N(\alpha, \beta) R |\xi|} - \frac{N(\alpha, \beta) R + \xi}{2} \times \ln \left| \frac{\sqrt{|\xi|} + \sqrt{N(\alpha, \beta) R}}{\sqrt{|\xi|} - \sqrt{N(\alpha, \beta) R}} \right| \right\}, \qquad \xi < 0. \tag{94}$$

Both functions $\kappa(\alpha)$ and $N(\alpha, \beta)$ are illustrated in figure 17.

There are many experimental results (Bouchaud *et al* 1990), Måløy *et al* 1992, Daguier *et al* 1996, 1997, Bouchaud 1997, 2003, Ponson *et al* 2006) that report the existence of a limiting roughness for the fracture surfaces. Considering these studies the practical range of fractal exponent is approximately $0.4 < \alpha < 0.5$. In the stability analysis we have used this range. The graph of the function $\kappa(\alpha)$ (we call it 'fractal constraint factor') is shown in figure 17 for the physically acceptable range of α. After some algebraic manipulations the following expression for $\kappa(\alpha)$ is obtained:

$$\kappa(\alpha) = -\frac{-1 + \alpha + (\alpha - 1)\mathrm{Im}\ ((-1)^{\alpha}(1 + \alpha))}{2\alpha(\alpha^2 - 1)} = \frac{1 + (\alpha - 1)\sin(\pi\alpha)}{2\alpha(1 - \alpha)}. \tag{95}$$

As stated earlier the function $\kappa(\alpha)$ relates the COD at the tip of a fractal crack to the COD at the tip of the corresponding smooth crack. Our studies show that for moderately rough cracks ($H > 0.8$) the COD within the whole cohesive zone can be approximated simply by multiplying the COD of the corresponding smooth crack by $\kappa(\alpha)$.

By moving the origin from the tip of the cohesive crack to the tip of the real crack and denoting the distance from the physical crack tip by x_1, the vertical displacement inside the cohesive zone of a fractal crack can be written as

$$v^{\mathrm{f}}[x_1, R^{\mathrm{f}}(x_1)] = \kappa(\alpha) \frac{4S}{\pi E'} \left[\sqrt{R^{\mathrm{f}}(x_1)\left[R^{\mathrm{f}}(x_1) - x_1\right]} - \frac{x_1}{2} \ln \left(\frac{\sqrt{R^{\mathrm{f}}(x_1)} + \sqrt{R^{\mathrm{f}}(x_1) - x_1}}{\sqrt{R^{\mathrm{f}}(x_1)} - \sqrt{R^{\mathrm{f}}(x_1) - x_1}} \right) \right], \tag{96}$$

for $0 < x_1 < R^{\mathrm{f}}$ and $R^{\mathrm{f}}(x_1) = N(\alpha, \beta) R(x_1)$.

A.3. Fractal loading parameter

Another important parameter in the stability analysis of fractal cracks is the loading parameter, which we denote by Q^{f}. When Wnuk's model of the structured cohesive zone is applied to study the stability problems associated with ductile fracture, the following relations will replace (48). First, it is noticed that for the small-scale yielding case, when the Barenblatt condition is satisfied, J-integral is directly proportional to the length of the cohesive zone R associated with a propagating crack; in the classic case when R is multiplied by a dimensionless constant $8S^2/\pi E'$, then one obtains J. Let us focus on $R^{\mathrm{f}}_{\mathrm{applied}}$. From the cohesive model of Dugdale–Barenblatt for a fractal crack it follows that

$$R^{\mathrm{f}}_{\mathrm{applied}} = \frac{(\alpha\pi^{1-\alpha})^{1/\alpha}}{2} \left[\frac{K_{\mathrm{I}}^{\mathrm{f(applied)}}}{S} \right]^{1/\alpha} = \frac{(\alpha\pi^{1-\alpha})^{1/\alpha}}{2} \left[\frac{\xi(\alpha)\sigma\sqrt{\pi a^{2\alpha}}}{S} \right]^{1/\alpha} = \frac{1}{2} a (Q^{\mathrm{f}})^{\frac{1}{\alpha}}. \tag{97}$$

The symbol Q^{f} is a non-dimensional loading parameter defined as

$$Q^{\mathrm{f}} = \frac{\alpha\sqrt{\pi}\Gamma(\alpha)}{\Gamma(1/2 + \alpha)} \frac{\sigma}{S}, \tag{98}$$

where σ is the applied stress and S is the cohesive strength. Because during all of the stable growth phase, according to equations (47) one has

$$R^{\mathrm{f}}_{\mathrm{applied}} = R^{\mathrm{f}}_{\mathrm{material}}, \tag{99}$$

we can drop the indices 'applied' and 'material', and simply use R. The derivatives $(\mathrm{d}R/\mathrm{d}a)_{\mathrm{applied}}$ and $(\mathrm{d}R/\mathrm{d}a)_{\mathrm{material}}$ must be computed. For the applied driving force expressed in terms of R as in (97), we have

$$\frac{\partial R^{\mathrm{f}}_{\mathrm{applied}}}{\partial a} = \frac{1}{2}(Q^{\mathrm{f}})^{\frac{1}{\alpha}} = \frac{R^{\mathrm{f}}_{\mathrm{applied}}}{a}. \tag{100}$$

In the non-dimensional form

$$\frac{\partial Y^{\mathrm{f}}_{\mathrm{applied}}}{\partial X} = \frac{Y^{\mathrm{f}}_{\mathrm{applied}}}{X} = \frac{Y^{\mathrm{f}}}{X(Y^{\mathrm{f}}, \rho, \alpha, \beta, X_0)}. \tag{101}$$

For the material resistance associated with quasi-static growth of a fractal crack the following expression was derived (see (62))

$$\frac{\mathrm{d}R^{\mathrm{f}}_{\mathrm{material}}}{\mathrm{d}a} = N(\alpha,\beta)F(R,\rho,\alpha,\beta), \tag{102}$$

where

$$F(R,\rho,\alpha,\beta) = \frac{1}{N(\alpha,\beta)}\left[M(\rho) - \frac{N(\alpha,\beta)R}{\Delta} + \sqrt{\frac{N(\alpha,\beta)R}{\Delta}\left(\frac{N(\alpha,\beta)R}{\Delta}-1\right)} - \frac{1}{2}\ln\left(\frac{\sqrt{\frac{N(\alpha,\beta)R}{\Delta}}+\sqrt{\frac{N(\alpha,\beta)R}{\Delta}-1}}{\sqrt{\frac{N(\alpha,\beta)R}{\Delta}}-\sqrt{\frac{N(\alpha,\beta)R}{\Delta}-1}}\right)\right]. \tag{103}$$

In its equivalent non-dimensional form the above equation reads

$$\frac{\mathrm{d}Y}{\mathrm{d}X} = F(Y,\rho,\alpha,\beta(X)), \tag{104}$$

in which the function F is defined in (68). The simplified versions of this equation was obtained for $\rho \gg 1$, and in order to use it one only needs to replace F by RF, see (74) and (75). The derivations of the functions F and RF are described in section 5, while the non-dimensional length of the cohesive zone and the non-dimensional crack length are defined as $Y = R/R_{\mathrm{initial}}$ and $X = a/R_{\mathrm{initial}}$. The material constant ρ is defined as $R_{\mathrm{initial}}/\Delta$ or $1+\varepsilon^{\mathrm{pl}}_{\mathrm{f}}/\varepsilon_0$, and it is named 'ductility index' as suggested by Wnuk and Mura (1981). For brittle materials ρ is close to one, while for ductile solids $\rho \gg 1$. The other parameter α denotes the fractality exponent, related to the dimension of the fractal representing a rough crack, and it is used here as a measure of the degree of roughness of the crack surfaces.

The loading parameter $\beta = \sigma/S$ is a function of the current crack length X during the entire process of subcritical crack growth, and it needs to be determined. There is no restriction on the values of β per se, but when we are studying the subcritical growth process, the condition $R^{\mathrm{f}}_{\mathrm{applied}} = R^{\mathrm{f}}_{\mathrm{material}}$ should be satisfied at every instant of the process and therefore β will become a function of X. By the use of (98), (100) and (101) we reach the following expression for β during the subcritical growth:

$$\beta(X) = \frac{\Gamma(1/2+\alpha)}{\alpha\sqrt{\pi}\Gamma(\alpha)}\left[\frac{2Y(X)}{X}\right]^{\alpha} N(\alpha,\beta(X))^{\alpha}. \tag{105}$$

If we substitute $N(\alpha,\beta(X))$ from (90) in the above equation after some algebraic manipulations, we reach the following well-known equation for the stress ratio during the subcritical crack growth phase under small-scale yielding restriction

$$\beta(X) = \frac{2}{\pi}\left[\frac{2Y(X)}{X}\right]^{1/2}. \tag{106}$$

It is seen that β for the fractal case is identical in form to that for the smooth case. However, it should be noted that the nominal crack length at the end of stable crack growth phase X_{f} explicitly depends on α and hence roughness of the crack affects the results for stress ratio during the subcritical growth of rough cracks (see figures 8 and 9). Another parameter required in the calculations is the length of the cohesive zone at the onset of crack growth R_{initial} corresponding to the requirement $K = K_{\mathrm{c}}$, and used as the normalizing constant for both R and a.

A.4. Motion of a subcritical fractal crack

To describe the slow motion of a subcritical crack, its length X is used as a time-like variable. Therefore, all pertinent quantities such as the applied load β (or Q) and the material toughness Y should be viewed as certain functions of X, namely $\beta = \beta(X)$, $Q = Q(X)$ and $Y = Y(X)$. During the stable crack extension the equalities described in (47) must be satisfied. Consistent with notation used here conditions (47) read

$$\tfrac{1}{2}Q(X)^2X = D(\alpha)^2Y(X), \tag{107}$$

where

$$D(\alpha) = \frac{2\alpha\Gamma(\alpha)}{\sqrt{\pi}\Gamma(1/2+\alpha)}. \tag{108}$$

Now with Q replaced by β, we can write

$$\frac{\pi^2}{8}\beta(X)^2X = Y(X). \tag{109}$$

Equations (107) and (109) are set up in such a way that the external effort or 'crack driving force' is placed on the left-hand side, while the quantity shown on the right-hand side represents non-dimensional material resistance to fracture. As can readily be seen, this resistance is not constant, as it is commonly assumed in the classical formulations of fracture mechanics; it is a certain function of the current crack length, and it varies within the range Y_{initial} and $Y_{\mathrm{f}} > Y_{\mathrm{initial}}$. The extent of this interval depends on the tearing modulus of the cracked solid. For a smooth crack the initially unknown function $Y = Y(X)$ can be determined from the governing differential equation of Wnuk–Rice–Sorensen (77). For SCG to occur the tearing modulus $\overline{M}$ has to exceed the minimum modulus M_{minimum}, which is a known function of material ductility index ρ, namely $1/2 + 1/2\ln(4\rho)$, cf Wnuk (1972). The material ductility index has been related by Wnuk and Mura (1981) to the yield strain ϵ_{Y} and the plastic component of the strain at fracture $\epsilon^{\mathrm{f}}_{\mathrm{pl}}$; $\rho = 1 + \epsilon^{\mathrm{f}}_{\mathrm{pl}}/\epsilon_{\mathrm{Y}}$. In this study we have suggested an extension of the governing equation (77) valid for a fractal crack, see (82) and (83). The governing differential equation for the case of a fractal crack reads

$$\frac{\mathrm{d}Y}{\mathrm{d}X} = F(X,\rho,\alpha,\beta(X)), \tag{110}$$

for an arbitrary value of the ductility index ρ, and

$$\frac{\mathrm{d}Y}{\mathrm{d}X} = RF(X,\rho,\alpha,\beta(X)), \tag{111}$$

for ductile materials for which $\rho \gg 1$. Functions F and RF have been defined in terms of the roughness measure α and the material ductility index ρ, cf section 7.

At the end of the SCG phase, when the terminal instability occurs, it is required that in addition to conditions (107) or (109) certain additional conditions are satisfied. To set up these conditions one needs to compare the second derivatives of the elastic potential of the cracked body and that of the corresponding entity representing material resistance, see (48). In terms of the non-dimensional functions this statement can be expressed as given in (82) and (83). These equations allow one to determine the set of critical values of crack length X_f and material toughness Y_f prevailing at the point of terminal instability. Numerical solutions to these equations have been found and they are best illustrated by the graphs depicted in figure 12. To establish the state of the terminal instability a technique of 'intersecting curves' has been used, see section 6 for the analysis and figure 12 for a graphical interpretation.

In closing we outline an alternative approach useful in the analysis pertinent to predicting the terminal instability. As the state of the terminal instability is approached, the slope of the Q versus X (or β versus X) curves tends to zero. Using (107), $Q(X)^2 = 2D(\alpha)^2 Y(X)/X$ and differentiating both sides of this equation (prime denotes the derivative with respect to X) we obtain $2Q\mathrm{d}Q = D(\alpha)^2(2XY' - 2Y)\mathrm{d}X/X^2$. Therefore, the derivative $\mathrm{d}Q/\mathrm{d}X$ (or $\mathrm{d}\beta/\mathrm{d}X$) is readily determined as

$$\frac{\mathrm{d}Q}{\mathrm{d}X} = D(\alpha)^2 \frac{XY' - Y}{X^2 Q}. \tag{112}$$

Replacing Y' by either F or RF provided in the governing equations (82) and (83) and setting $dQ/\mathrm{d}X$ equal to zero, yields two simple equations equivalent to (82) and (83)

$$\begin{aligned} &F(Y(X), \rho, \alpha, \beta(X))X - Y(X) = 0 \qquad \text{(arbitrary } \rho\text{)}, \\ &RF(Y(X), \rho, \alpha, \beta(X))X - Y(X) = 0 \qquad (\rho \gg 1). \end{aligned} \tag{113}$$

We were unable to find closed-form solutions to these equations and thus some numerical solutions are provided instead. Effects of the roughness of crack surfaces, material ductility, and the initial crack size on the characteristic parameters describing the state of the terminal instability have been demonstrated graphically; see figures 13, 14 and 15.

References

Alves L M, Silva R V and Lacerda L A 2010 *Eng. Fract. Mech.* **77** 2451–66

Anderson T L 2004 *Fracture Mechanics: Fundamentals and Applications* 2nd edn (Boca Raton, FL: CRC Press)

Balankin A S 1997 *Eng. Fract. Mech.* **57** 135–207

Barenblatt G I 1962 *Advances in Applied Mechanics* vol VII (New York: Academic) pp 55–129

Borodich F M 1997 *J. Mech. Phys. Solids* **45** 239–59

Bouchaud E, Lapasset G and Planès J 1990 *Europhys. Lett.* **13** 73–9

Bouchaud E 1997 *J. Phys.: Condens. Matter* **9** 4319

Bouchaud E 2003 *Surf. Rev. Lett.* **10** 797–814

Budiansky B 1988 *Universal R-curve for Ductile Materials* (Cambridge, MA: Harvard School of Engineering and Applied Sciences)

Burdekin F M and Stone D E W 1966 *J. Strain Anal.* **1** 145–53

Carpinteri A 1994 *Int. J. Solids Struct.* **31** 291–302

Carpinteri A and Chiaia B 1996 *Int. J. Fract.* **76** 327–40

Cherepanov G P, Balankin A S and Ivanova V S 1995 *Eng. Fract. Mech.* **51** 997–1033

Daguier P, Henaux S, Bouchaud E and Creuzet F 1996 *Phys. Rev.* E **53** 5637–42

Daguier P, Nghiem B, Bouchaud E and Creuzet F 1997 *Phys. Rev. Lett.* **78** 1062–64

Erdogan F 1962 *Proc. 4th US National Congress on Applied Mechanics (Berkeley, CA)* p 547

Gol'dshteĭn R V and Mosolov A B 1991 *Sov. Phys. Dokl.* **36** 603–5

Gol'dshteĭn R V and Mosolov A B 1992 *J. Appl. Math. Mech.* **56** 563–71

Griffith A A 1921 *Phil. Trans. R. Soc. Lond.* A **221** 163–98

Gross D 1990 *Nonlinear Fracture Mechanics* (*CISM Courses and Lectures* No 314) (Berlin: Springer)

Hult J A and McClintock F A 1956 *Proc. 9th Int. Congress of Applied Mechanics* vol 8 (Brussels) pp 51–8

Hutchinson J W and Paris P C 1977 *Proc. ASTM Symp. on Elastic-Plastic Fracture (Atlanta, GA)* (Philadelphia, PA: American Society for Testing and Materials) (published as an ASTM-STP Report)

Irwin G R 1957 *J. Appl. Mech.* **24** 361–4

Irwin G R 1958 *Fracture, Handbook der Physik* (Berlin: Springer) vol VI, pp 551–90

Irwin G R, Lingaraju B and Tada H 1969 *Fritz Engr. Lab. Report No* 358-2, Lehigh University

Krafft J M, Sullivan A M and Boyle R W 1961 *Proc. Crack Propagation Symp.* (Cranfield, England: Cranfield College of Aeronautics)

Le J L, Bažant Z P and Bažant M 2009 *J. Phys. D: Appl. Phys.* **42** 214008

Måløy K J, Hansen A, Hinrichsen E L and Roux S 1992 *Phys. Rev. Lett.* **68** 213–15

Mandelbrot B B, Passoja D E and Paullay A J 1984 *Nature* **308** 721–22

McClintock F A 1958 *J. Appl. Mech.* **25** 582–88

McClintock F A and Irwin G R 1965 *Fracture Testing and its Applications* STP vol 381 (Philadelphia, PA: ASTM) pp 84–113

Michel B 1991 *Proc. Int. Summer School on Fracture Mechanics, IFMASS 6, and European Structural Integrity Society (ESIS) Service Cracks in Pressure Vessels & Storage Tanks, 6th Int. Fracture Mechanics Summer School (IFMASS 6)* (*Vrdnik, Yugoslavia*)

Mosolov A B 1991 *Dokl. Akad. Nauk SSSR* **319** 840–4

Muskhelishvili N I 1933 *Some Basic Problems of Mathematical Theory of Elasticity* (Published in Russian in (1933) (Leyden, The Netherlands: Noordhoff International Publishing) (English translation) (1953))

Paris P C and Sih G C 1965 *Fracture Toughness Testing and its Applications* vol 381 (Philadelphia, PA: ASTM) pp 30–83

Paris P C, Tada H, Zahoor A and Ernst H 1977 *US Nuclear Regularity Commission Report NUREG-0311* (available through National Technical Information Service, Springfield, VA)

Ponson L *et al* 2006 *Int. J. Fract.* **140** 27–37

Pugno N and Ruoff R S 2004 *Phil. Mag.* **84** 2829–45

Rice J R 1968 *Mathematical Analysis in the Mechanics of Fracture, Fracture, An Advanced Treatise* vol II, ed H Liebowitz (New York: Academic)

Rice J R and Sorensen E P 1978 *J. Mech. Phys. Solids* **26** 163–86

Rice J R, Drugan W J and Sham T L 1980 *Fracture Mechanics: 12th Conf. (Philadelphia) ASTM STP 700* pp 189–221

Sih G C 1962 *Trans. Chin. Assoc. Adv. Stud.* **25** 25–35

Sih G C 1964 *Proc. 2nd Conf. on Theoretical and Applied Mechanics (New York)* (New York: Pergamon) p 117

Slater L J 2008 *Generalized Hypergeometric Functions* reissue edn (Cambridge: Cambridge University Press)

Tada H, Paris P C and Irwin P C 1985 *The Stress Analysis of Cracks Handbook* 2nd edn (St. Louis, MO: Paris Production Incorporated (and Del Research Corporation))

Taylor D, Cornetti P and Pugno N 2005 *Eng. Fract. Mech.* **72** 1021–38
Weisstein E W 2003 *CRC Concise Encyclopedia of Mathematics* 2nd edn (Boca Raton, FL: CRC Press)
Wells A A 1963 *Bri. Weld. J.* **10** 563–70
Westergaard H M 1939 *J. Appl. Mech.* **66** A49–53
Williams M L 1957 *ASME J. Appl. Mech.* **24** 109–14
Wnuk M P 1972 *Proc. Int. Conf. on Dynamic Crack Propagation* ed G C Sih Lehigh University (Leyden, The Netherlands: Noordhoff) pp 273–80
Wnuk M P 1974 *J. Appl. Mech.* **41** 234–42
Wnuk M P 1990 *Nonlinear Fracture Mechanics* (*CISM Courses and Lectures* No 314) (Berlin: Springer)
Wnuk M P and Knauss W G 1970 *Int. J. Solids Struct.* **6** 995–1009
Wnuk M P and Legat J 2002 *Int. J. Fract.* **114** 29–46
Wnuk M P and Mura T 1981 *Int. J. Fract.* **17** 493–517
Wnuk M P and Mura T 1983 *Mech. Mater.* **2** 33–46
Wnuk M P and Yavari A 2003 *Eng. Fract. Mech.* **70** 1659–74
Wnuk M P and Yavari A 2005 *Eng. Fract. Mech.* **72** 2744–57
Wnuk M P and Yavari A 2008 *Eng. Fract. Mech.* **75** 1127–42
Wnuk M P and Yavari A 2009 *Eng. Fract. Mech.* **76** 548–59
Xie H 1989 *Int. J. Fract.* **41** 267–74
Yavari A 2002 *Fractals* **10** 189–98
Yavari A and Khezrzadeh H 2010 *Eng. Fract. Mech.* **77** 1516–26
Yavari A, Hockett K G and Sarkani S 2000 *Int. J. Fract.* **101** 365–84
Yavari A, Sarkani S and Moyer E T 2002a *Int. J. Fract.* **114** 1–27
Yavari A, Sarkani S and Moyer E T 2002b *J. Appl. Mech.* **69** 45–54